

**CHARACTERIZATION AND COMPARISON ON PHENOTYPIC  
DIFFERENCES OF VACCINE AND CIRCULATING STRAINS  
OF INFLUENZA B VIRUSES IN B/VICTORIA AND  
B/YAMAGATA LINEAGES IN THE 2017-18 SEASON**

by  
Ruifeng Zhou

A thesis submitted to Johns Hopkins University in conformity with the requirements for the  
degree of Master of Science

Baltimore, Maryland

April 2021

## Abstract

Influenza in the human population is mainly caused by infection with influenza A viruses (IAVs) and influenza B viruses (IBVs). Although pandemic influenza is only caused by IAV, IBV is detected at increasing rates in seasonal influenza. IBV is divided into two antigenically and genetically distinct lineages, B/Yamagata and B/Victoria based on the hemagglutinin (HA) protein. Annual influenza vaccines include both IBV lineages in the quadrivalent vaccines and induce strain-specific protection. Vaccine production traditionally involved passaging viruses in embryonated eggs. More recent manufacturing techniques use cell culture-based methods which can increase virus production and possibly reduce the risk of antigenic changes by egg adaptation. Both egg and cell adaptation have been extensively studied in IAV, but comparable research in IBV is not abundant. We hypothesized that egg and cell culture adaptation also happen in IBV, and the changes lead to alteration of replication fitness in primary human epithelial cell cultures. To test this hypothesis, I focused on characterizing the phenotypic differences between vaccine and circulating strains of IBV in the B/Victoria and B/Yamagata lineages during the 2017-18 season. The results showed that the cell-derived vaccine strain had lower replication fitness in both lineages, but egg-derived vaccine strains had no observable phenotypic change compared to the circulating strains. Sequencing of the HA segment showed both cell and egg adaptation induced mutations in the HA. Egg adaptation caused a substitution at residue 197 which resulted in loss of a N-linked glycosylation site. Results from neutralization assays showed better recognition of egg-derived vaccine virus in the B/Yamagata lineage by both convalescent and post-vaccination human sera. These results suggested that cell and egg adaptations can cause viral fitness changes in IBV in cell culture and alter the antigenic profile of the virus. The possibility of antigenic changes causing vaccine mismatches needs to be considered during vaccine producing by the traditional egg method.

Primary Advisor/Reader: Dr. Andrew Pekosz, PhD

Secondary Reader: Dr. Sabra Klein, PhD

## Acknowledgment

I would like to thank Dr. Andrew Pekosz for the opportunity to work in this wonderful and collaborative lab. It was my first exposure to virology research, but his work on influenza viruses immediately got me interested in it. Dr. Pekosz has been very supportive and kind from my first day in the lab. His dedication, passion and knowledge in virology inspired me to keep pursuing a career in virology research. This thesis will also not be possible if not by Dr. Jo Wilson. She led the IBV studies in the lab before I joined and completed the neutralization assays in this thesis. I would also like to thank Jessica Resnick, Dr. Hsuan Liu, Allison Chen and Siddhant Vyas for training me various assays and instruments, and thank all other past and present lab members. Thank you to the ScM and PhD student cohort, especially Kirsten Littlefield and Patrick Creisher from the Klein lab. Also, a big thank you to the Klein and Davis lab for making suggestions in those joint lab meetings.

COVID-19 marked another great challenge in human history. I would like to say thank you to all the frontline medical workers and researchers who had been working hard to advance our understanding of this new coronavirus and rolling out vaccines at the pace never seen before in the history. I am also very proud to be a part of a SARS-CoV-2 study in hamsters thanks to the opportunity from Dr. Pekosz. This would be my small contribution back to the world during this pandemic.

Finally, I want to thank Yuyang Huang, Chengzhang Zhu, Qingwei Niu, Zhiyuan Huang and Haoyang Luo, my Chinese friends at JHSPH for supporting each other on a continent far away from home. Special thanks and congratulations to Jinke Wu who is graduating from JHU with me again this year, after we graduated from the same middle school, high school and college.

## Table of Contents

<b>Chapter 1. Introduction.....</b>	<b>1</b>
Influenza.....	1
Influenza B Virus.....	2
<i>Structure and Core Protein Function</i> .....	2
<i>Evolution and Host Range</i> .....	4
<i>Epidemiology</i> .....	6
<i>Vaccines</i> .....	7
<b>Hypothesis and Research Aims.....</b>	<b>12</b>
<b>Chapter 2. Identify IBV clinical isolates of the appropriate lineages from the 2016-17 and 2017-18 seasons.....</b>	<b>13</b>
Rationale.....	13
Materials and Methods.....	14
<i>Complete Media (CM)</i> .....	14
<i>Infection Media (IM)</i> .....	14
<i>PBS and PBS+</i> .....	15
<i>RT-PCR</i> .....	15
<i>MDCK-SIAT1 cell</i> .....	16
<i>hNEC cell culture</i> .....	16
<i>Generating virus stocks</i> .....	16
<i>Fifty percent tissue culture infectious dose (TCID<sub>50</sub>)</i> .....	17
<i>Flow cytometry</i> .....	17
Results.....	18
<i>Lineage identification of IBV clinical samples by RT-PCR</i> .....	18
<i>Passage of IBV clinical strains on hNEC culture and growing virus stocks</i> .....	19
<i>Flow cytometry to re-confirm the lineages of IBV clinical strains</i> .....	19
Discussion.....	20
<b>Chapter 3. Viral phenotype characterization of egg-adapted, cell-adapted vaccine strains and circulating strains from both lineages.....</b>	<b>24</b>
Rationale.....	24
Materials and Methods.....	25
<i>MDCK-SIAT1 cell</i> .....	25
<i>hNEC cell culture</i> .....	25
<i>Plaque assay</i> .....	26
<i>MDCK-SIAT1 growth curve</i> .....	26
<i>hNEC growth curve</i> .....	27
<i>Fifty percent tissue culture infectious dose (TCID<sub>50</sub>)</i> .....	27

Results .....	28
<i>Plaque morphology</i> .....	28
<i>Low MOI growth curve</i> .....	29
Discussion .....	30
<b>Chapter 4. Sequencing of HA segment and differential neutralizing antibody titers against vaccine and circulating strains .....</b>	<b>35</b>
Rationale .....	35
Materials and Methods.....	35
<i>RT-PCR</i> .....	35
<i>Sequencing</i> .....	36
<i>HA modeling</i> .....	36
Results .....	37
<i>RT-PCR of HA segment</i> .....	37
<i>Amino acid changes and mapping mutations on HA model</i> .....	37
<i>Differential neutralization titer to egg-derived vaccine virus compared to circulating strain</i> .....	38
Discussion .....	39
<b>Chapter 5. Conclusion and Future Direction .....</b>	<b>44</b>
<b>Appendix. SARS-CoV-2 Lung Pathology in Golden Syrian Hamsters .....</b>	<b>46</b>
Background.....	46
Materials and Methods.....	46
<i>Tissue homogenization</i> .....	46
<i>TCID<sub>50</sub></i> .....	47
Results .....	48
<i>Similar SARS-CoV-2 replication kinetics between sexes</i> .....	48
Discussion and Conclusion .....	48
<b>References .....</b>	<b>50</b>
<b>Curriculum Vitae .....</b>	<b>53</b>

## List of Tables

Table 1: All virus strains used in this thesis .....	14
Table 2: Sequences of primers used for lineage identification RT-PCR.....	16
Table 3: Sequences of PR-PCR primers and sequencing primers for IBV HA sequencing.....	36
Table 4: All amino acid changes in B/Victoria lineage .....	38
Table 5: All amino acid changes in the B/Yamagata lineage .....	38

## List of Figures

Figure 1.1: Structure of influenza B virus .....	9
Figure 1.2: Influenza positive tests reported to CDC by public health laboratories, national summary, 2017-18 season.....	9
Figure 1.3: Age group distribution of influenza B positive specimens reported by public health laboratories, national summary, 2017-18 season.....	10
Figure 1.4: Number of influenza-associated pediatric deaths by week of death.....	11
Figure 2.1: Gel image of RT-PCR products of IBV-positive NP swab samples from the 2017-18 flu season .....	22
Figure 2.2: Gel image of RT-PCR products of isolated plaques from plaque purification of NP swab sample 11-Pro-365.....	22
Figure 2.3: Gel image of RT-PCR products of IBV-positive NP swab samples from the 2016-17 flu season .....	23
Figure 2.4: Flow cytometry for IBV clinical strain lineage identification .....	23
Figure 3.1: Plaque Assays.....	33
Figure 3.2: Low MOI Growth Curves .....	34
Figure 4.1: Mutations mapped on IBV HA model .....	42
Figure 4.2: Neutralization assay .....	43
Figure A1. Infectious virus titers separated by sex in different hamster tissues .....	49



## Chapter 1. Introduction

### Influenza

Influenza (flu) is typically a seasonal respiratory disease usually peaks during winter. The two viruses that cause influenza in humans are Influenza A virus (IAV) and Influenza B virus (IBV) [1]. Influenza is contagious and is transmitted between people by aerosol droplets when infected individuals cough, sneeze or talk [2]. Influenza virus infection can cause mild to severe disease, even death. Typical symptoms include fever, cough, headache, sore throat, muscle ache, fatigue, etc. [2]. Influenza is considered a major public health burden in the world. It is estimated that the average incidence rate of symptomatic influenza is 8% between 2010 to 2016 in the US and varied from 3% to 11% between seasons [3]. Many factors contribute to the burden of influenza in the US every year, including virus strains, timing of season, vaccine efficacy and coverage [4]. The preliminary analysis by CDC estimates that influenza causes 9 - 45 million annual total illnesses, 140,000 – 810,000 hospitalization and 12,000 – 61,000 deaths in the US since 2010 [4].

Since influenza symptoms are similar to other respiratory illnesses, it is impossible to diagnose accurately for influenza by symptoms alone. Laboratory tests are needed to confirm infection with influenza virus. Rapid Influenza Diagnostic Tests (RIDTs) are the most common tests carried out for diagnosis of influenza in the US [5]. It is an antigen test that detects nucleoproteins of both IAV and IBV in specimens [6]. RIDT is rapid and does not require extensive laboratory expertise to perform, but they have lower sensitivity compared to the reference standards for lab confirmation of influenza virus which are reverse transcription-

polymerase chain reaction (RT-PCR) or viral culture [6]. The RT-PCR test is a molecular assay that detects viral RNA in patient samples. Since residual viral RNA can still be present in patients' respiratory track, a positive result by RT-PCR does not necessarily mean infectious virus production or ongoing illness [7].

## Influenza B Virus

### *Structure and Core Protein Function*

Influenza B virus, like IAV, belongs to the *Orthomyxoviridae* family. The IBV virion is enveloped. It has a segmented genome consisting of 8 single-stranded RNAs (Figure 1.1). The 8 segments - in order of their lengths: PB1, PB2, PA, HA, NP, NB/NA, M1/BM2 and NS1/NEP - encode for 11 proteins by mechanisms including alternative open reading frame utilization and alternative spliced mRNA [8]. The IBV genome encodes 6 fewer proteins than IAV [8, 9], lacking accessory proteins such as PB1-F2, PB1-N40, PA-X, PA-N155, PA-N182, M43 and NS3, it does encode unique proteins not found in IAV like NB and BM2 [10, 11].

The hemagglutinin (HA) is one of the 3 integral membrane proteins in IBV. This glycoprotein consists of 3 identical monomers and mediates receptor binding on cell surface and membrane fusion in the endosome [10, 12, 13]. IBV HA shares similar overall structure to IAV HA, although the sequence homology is low [10]. Sialic acids are the surface receptors used by influenza viruses. In the human upper respiratory track, epithelial cells predominantly express  $\alpha$ -2,6-linked sialic acids, while  $\alpha$ -2,3-linked sialic acids are more common in the lower respiratory tract. IBV HA has higher affinity to  $\alpha$ -2,6-linked sialic acids, although it can bind both forms [10, 14]. The HA is cleaved into 2 separate polypeptide chains during processing. HA1 is the

globular glycoprotein head and contains the receptor binding domain (RBD). HA2 is the stalk/stem core and contains the fusion peptide [12, 15]. Upon receptor binding, the virion is endocytosed into the endosome. Lowering of endosomal pH causes conformational changes in HA, insertion of the fusion peptide into the endosomal membrane, followed by membrane fusion [12, 13, 15, 16]. Meanwhile, the membrane protein BM2, analogous to the M2 proton channel in IAV, acidifies the internal space of the virion, causing uncoating and facilitating the release of viral ribonucleoprotein (RNP) into the host cytoplasm [8, 15, 16].

The neuraminidase (NA) is another IBV surface protein that is responsible for cleavage of sialic acids on the cell surface and release of newly produced virions [10, 12]. NA is a tetramer of identical subunits [12]. While the IBV and IAV NA have very low overall sequence homology, both contain active sites consisting of 19 highly conserved residues, and share similar overall structures [10].

PA, PB1 and PB2 form the polymerase complex of IBV. Despite minimal data on their exact function in IBV, they are thought to work similarly to the polymerase in IAV [10]. Influenza virus has a negative sense genome, so the RNA-dependent RNA polymerase (RdRp) must produce positive sense mRNA immediately upon entry into the cell. The RdRp in an assembled virion is bound to each segment of genomic RNA in the viral RNP structure. Upon uncoating, the vRNP is transported into the nucleus for viral replication. Two main advantages of replication in the nucleus are that there is a lower chance of being detected by innate immune sensors in the cytoplasm, and the RdRp can snap the 5' phosphate caps from host mRNA [15-17].

The NB protein is unique to IBV. It is encoded by the NA segment but 4 nucleotides upstream of the NA start codon [10]. It is shown to be an integral component of IBV membrane

and possess ion channel activity [18-21]. However, the exact function of this protein is unknown.

### *Evolution and Host Range*

The first strain of IBV was isolated in 1940 [22] and IBV diverged into 2 genetically distinct lineages, B/Victoria and B/Yamagata, some time before 1983 [8, 10, 23]. The two lineages are defined by their HA sequences, in contrast to IAV where subtypes are characterized by both HA and NA sequences [8, 10, 16]. IBV cases in each season had been dominated by a single lineage prior to 2001. Since the reappearance of B/Victoria in 2002, the two lineages of IBV have been co-circulating with the two IAV subtypes [8, 10, 24, 25]. Apart from possible intrinsic viral factors, the dominance of a lineage in a season can also be influenced by external factors like vaccine efficacy and vaccine composition. Different evolutionary patterns are observed between the two lineages with B/Yamagata evolving into multiple clades that co-circulate, while B/Victoria viruses follow a more linear evolutionary pattern with the newer clades often replacing the previous ones [8, 10, 24].

IBV is also subjected to antigenic drift, although the rate of nucleotide substitution is lower than that in IAV. Both the HA and NA segments experience high adaptive evolution with HA segment being the highest [8, 10, 24, 26]. Antigenic drift is gradual changes on the virus as they replicate which eliminate antibody binding epitopes, allowing for escape from pre-existing immunity. The mutations can be additions, deletions or substitutions of nucleotides. These errors are caused by RdRp in IBV, which like in many other RNA viruses, lacks proof-reading function. In a single infected cell, thousands of copies of genomes can be generated which may contain mutations. Newly packaged virions with these mutations can infect other cells in the same host or be transmitted to another host and continue to accumulate mutations. The resulting mutation rate is around  $2.0 \times 10^{-3}$  substitutions per site per year in IBV [24, 26]. Drifts on HA

can gradually change the antigenic profile of the virus. Nonsynonymous mutations are especially frequent near RBD [8]. This can result in evasion of neutralization by antibody and emergence of new strains.

Reassortment is another way in which IBV can acquire genetic variation [24, 26]. The influenza virus genome is segmented and when a single cell is co-infected by two or more viruses, their genetic material can be exchanged by segment reassortment. This is a strategy which can introduce a larger degree of genome diversity in a short period of time because it involves changes in an entire segment, as opposed to accumulating single mutations. Antigenic shift is well documented in IAV as the major cause of multiple pandemic influenza outbreaks [27, 28]. While human IAV primarily use  $\alpha$ -2,6-linked sialic acids as receptor, avian influenza viruses primarily bind to  $\alpha$ -2,3-linked sialic acids. Pigs which express both  $\alpha$ -2,3- and  $\alpha$ -2,6-linked sialic acids, can be co-infected by human and avian flu. Segments from the two strains can reassort and the resulting virus may cross species barriers and infect human. Humans have no pre-established immunity against these new strains which potentially cause pandemic outbreaks.

IBV is strictly a human pathogen, meaning there is no known natural animal reservoirs [8, 10] and only occasional detection of IBV in seals, pigs and dogs [29-31]. Unlike IAV, which has a wide range of natural hosts, IBV has no risk of constant spill over to humans from animal hosts or antigenic shifts, although reassortment between viruses of the same lineage or viruses of the two separate lineages has been observed [8]. A study in China showed B/Yamagata-B/Victoria inter-lineage reassortment occurred in 2013-14 season [32]. New strains were formed from B/Yamagata HA in 2013-14 season and B/Victoria NA in 2011-12 season.

## *Epidemiology*

Influenza B Viruses are increasingly becoming prominent contributors to the global burden of influenza. Since 2000s, B/Yamagata and B/Victoria lineages have been co-circulating with IAV subtypes H1N1 and H3N2 in human populations [8, 10, 33, 34]. IBV was responsible for a median 23.4% of total reported influenza cases in 31 countries world-wide from 2000 to 2018. IBV epidemics usually peak 0.6 – 1.1 months later than IAV [34]. The 2017-18 season, which is the season of interest in this thesis, is shown as an example in Figure 1.2 [35]. Most of the cases in this particular season were dominated by IAV, and IBV cases peaked around 4 weeks later than IAV. Interestingly, the 2019-2020 flu season had an early rise of IBV cases parallel to the rise in IAV. There were also significantly more IBV cases compared to previous flu seasons [35].

Although IBV is capable of infecting people through a wide range of age, older children and young adults appear to be most susceptible to IBV. Disease manifestations are more prevalent in younger populations [10]. IBV causes out of proportion pediatric deaths compared to IAV. CDC reported that except for the 2009 pandemic year, between 2004 and 2011 IBV caused 34% of influenza-associated deaths in pediatric population [10, 36]. It is also interesting to note that B/Victoria seems to be more prevalent in younger populations than B/Yamagata [8, 10]. If we look at cases by age from the 2017-18 season, more IBV cases appeared in younger age groups. Patients between 5-24 years of age saw the highest proportion of IBV cases (Figure 1.3) [37]. The 2019-20 season also saw the highest proportion of pediatric deaths caused by IBV, followed by the 2017-18 season from year 2016 to 2020 (Figure 1.4) [36].

## *Vaccines*

Annual influenza vaccines for IBV are widely available in the world. There are two main types of flu vaccines, inactivated flu vaccine and live-attenuated flu vaccine. The US uses quadrivalent vaccine which includes both subtypes of IAV and both lineages of IBV [38]. Vaccines against IBV provide lineage-specific protection, since the two lineages are antigenically distinct. Neutralizing antibodies typically bind to HA on IBV, which interferes with protein binding to cell surface receptors and subsequent fusion between the virus and host membranes. For the vaccine to work, the HA in the influenza vaccine has to antigenically match the HA in circulating IBV strains. A big challenge in influenza vaccine manufacturing is that candidate strains must be selected before the start of season which the vaccine will be distributed. Traditional influenza vaccines are manufactured in embryonated hen's eggs. Viruses are injected into the allantoic cavity and allowed several passages to produce large amount of virus stocks to be made into vaccines. The process is lengthy and requires a large number of eggs and facilities to harvest, inactivate and partially purify the virus. The surveillance and tracking of influenza activity provide insights into what strains should be chosen for the next influenza season [25].

Since candidate strains are selected before the season starts, there is a possibility of vaccine mismatches. A mismatched vaccine has an HA protein which has different antigenic properties to the circulating strains. Neutralizing antibodies generated against the vaccine strain may not be effective in inhibiting the circulating strain, decreasing vaccine efficacy. Another way for vaccine mismatch to happen is through the egg-adaptation process itself. This process is well documented in IAV [39-41], and IBV [42, 43]. Recently, the FDA approved flu vaccine manufacturing using cell-based techniques. However, prior of the 2019-2020 flu season, some of

the virus strains provided for cell-based production were still derived in eggs. When a virus is passaged in non-primary cell cultures, there is a possibility that mutations can be selected for which provide the virus with a replication advantage. The adaptation of IAV or IBV to embryonated eggs or to cell lines may select for viruses with a fitness advantage over the parental strains, and these strains would then go on to be used in the vaccine manufacturing process. Previous research has shown that point mutations on the HA protein were induced on B/Victoria viruses when adapting to embryonated hen's eggs. These mutations shifted the virus's preference from  $\alpha$ -2,6- to  $\alpha$ -2,3-linked sialic acids, and helped the virus to grow to a higher titer than wildtype strains [44, 45]. It is also possible for the virus to acquire mutations near RBD on the HA protein where neutralizing antibodies bind and alter its antigenic sites. A study reported that antibodies binding more efficiently to egg-adapted H1N1 HA than to wildtype H1N1 HA were found in about 5% of vaccinated individuals in the 2015-16 season [46]. In the 2016-17 season, the lack of a glycosylation site on the HA of egg-adapted H3N2 vaccine strain contributed to a low vaccine efficacy [47]. This poses a concern for vaccine production as the resulting vaccine strain may not well represent the circulating strain in the flu season, thus causing vaccine mismatches.



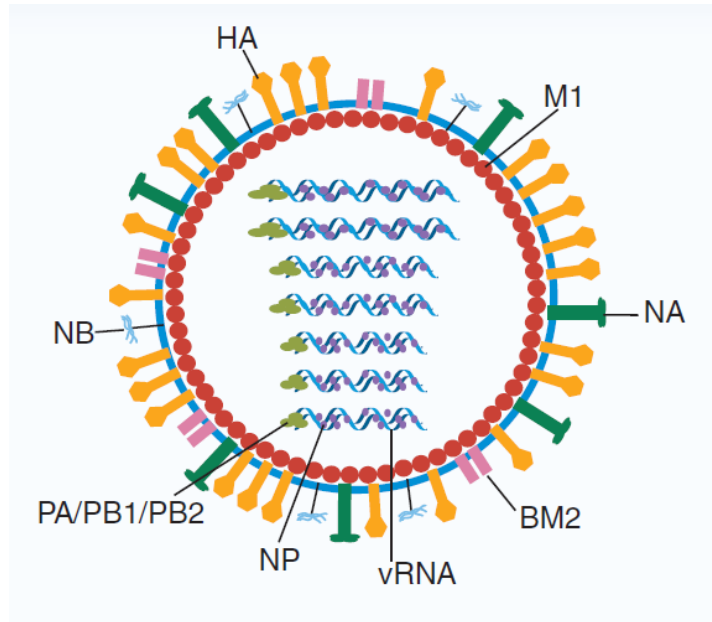


**Figure 1.1: Structure of influenza B virus.** Koutsakos et al., 2016 [10]



Influenza Positive Tests Reported to CDC by Public Health Laboratories, National Summary, 2017-18 Season, week ending Sep 29, 2018

Reported by: U.S. WHO/NREVSS Collaborating Laboratories and ILINet

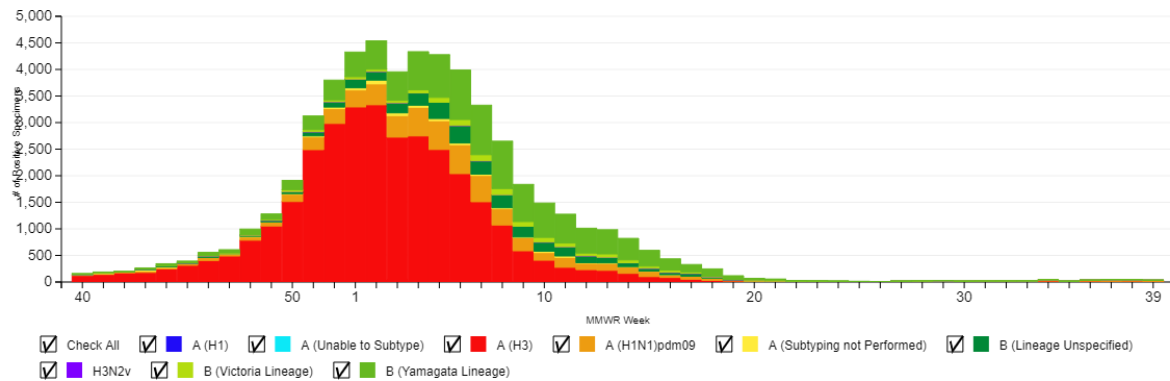


**Figure 1.2: Influenza positive tests reported to CDC by public health laboratories, national summary, 2017-18 season.** CDC, 2018 [35]

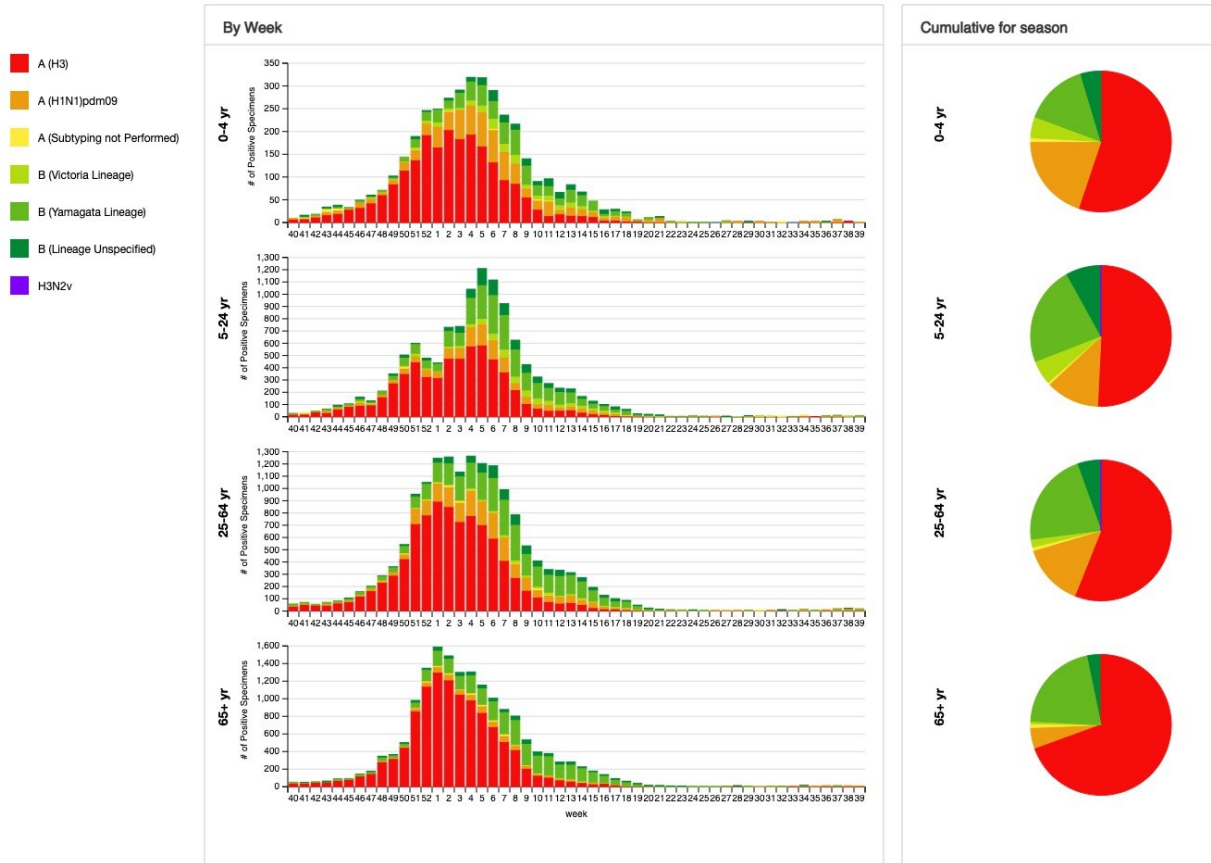


**Figure 1.3: Age group distribution of influenza B positive specimens reported by public health laboratories, national summary, 2017-18 season. CDC, 2018 [37]**

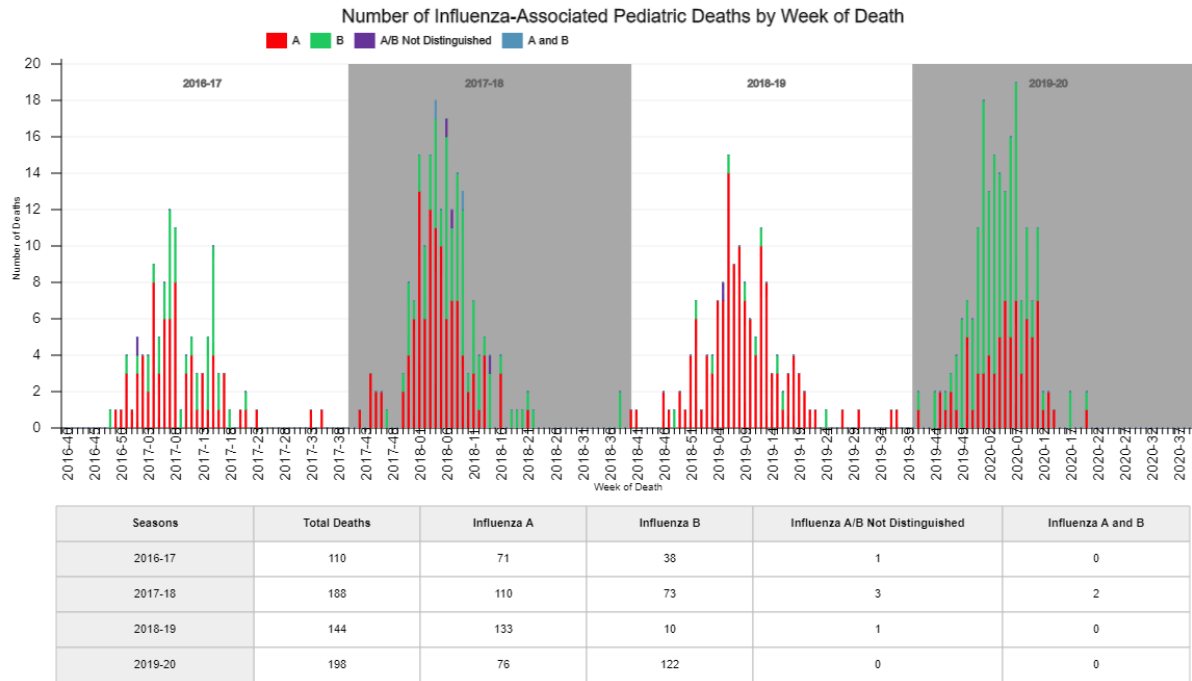


**Figure 1.4: Number of influenza-associated pediatric deaths by week of death. CDC, 2020 [36]**

## **Hypothesis and Research Aims**

Influenza A viruses have been well studied historically. While causing significant a number of cases each year worldwide, Influenza B virus is generally less well studied. I hypothesize that egg and cell culture adaption of IBV leads to changes that will alter the replication of the virus in primary human nasal epithelial cell cultures. To test this hypothesis, my research has focused on the characterization and comparison of phenotypic differences between vaccine and circulating strains of IBV in the B/Victoria and B/Yamagata lineages during the 2017-18 season.

The thesis is broken down into the following chapters:

1. Isolation of circulating strains of both lineages
2. Characterization of circulating strains, egg-cultured vaccine strains and cell-cultured vaccine strains with comparisons between circulating and vaccine strains of the same lineage, and between circulating strains from the two lineages.
3. Sequencing of HA segments to identify potential mutations which cause the phenotypic differences between strains.

## **Chapter 2. Identify IBV clinical isolates of the appropriate lineages from the 2016-17 and 2017-18 seasons**

### **Rationale**

My initial goal was to identify the appropriate IBV circulating strains from The Johns Hopkins Center for Excellence in Influenza Research and Surveillance (JH-CEIRS) sample inventory. Nasopharyngeal swab samples were collected from patients who visited Johns Hopkins Hospital. Samples tested positive for IBV infection were requested from the JH-CEIRS repository. They were then screened for IBV lineage, and selected strains were used to grow working stocks.

RT-PCR is the standard lab test for IBV lineage identification. Since the two lineages of IBV, B/Yamagata and B/Victoria, have genetically distinct HA segments, the lineage of a clinical strain can be determined by RT-PCR using two sets of lineage-specific primers. The isolated vRNA was amplified using WHO recommended primers for IBV lineage identification. The cDNA product generated from B/Yamagata and B/Victoria viruses would be about 388bps and 284bps, respectively.

After lineage screening, swab samples were put on human nasal epithelial cell (hNEC) culture. This was to amplify any infectious virus present in those samples. hNEC cultures are a primary cell culture system that faithfully reproduces the cells that are present in the upper respiratory tract and are targeted by influenza viruses. As a result, passaging in these cultures would be less likely to cause mutations which could change the virus phenotype. After we

initially amplified IBV stocks in hNEC cultures, MDCK-SIAT1 cells were used for growing virus stocks. Madin-Darby Canine Kidney (MDCK) cells are the most widely used cell line for lab research on influenza virus. They are easy to culture and can be infected by many influenza viruses. They have both  $\alpha$ -2,3- and  $\alpha$ -2,6-linked sialic acids although  $\alpha$ -2,3-linked sialic acids are predominantly expressed. MDCK-SIAT1 cells were derived from a MDCK cell line with stable transfection of a cDNA encoding human 2,6-sialyltransferase (SIAT1) [48]. MDCK-SIAT1 cells express more  $\alpha$ -2,6-linked sialic acids and are more suitable to support IBV infection.

Virus strain names and lineages used in this and following chapters are listed here:

	<b>B/Yamagata</b>	<b>B/Victoria</b>
Circulating strains	B/Baltimore/R0250/2018 B/Baltimore/R0300/2018	B/Baltimore/R0001/2016 B/Baltimore/R0122/2016
Egg-derived vaccine strain	B/Phuket/3073/2013 egg	B/Colorado/06/2017 egg
Cell-derived vaccine strain	B/Phuket/3073/2013 cell	B/Iowa/06/2017 cell

Table 1: All virus strains used in this thesis.

## Materials and Methods

### *Complete Media (CM)*

Dulbecco's Modified Eagle Media (DMEM) supplemented with 10% by volume fetal bovine serum (FBS), 2mM GlutaMAX, 100U/mL penicillin, and 100ug/mL of streptomycin were used as complete growth media for MDCK-SIAT1 cells.

### *Infection Media (IM)*

Dulbecco's Modified Eagle Media (DMEM) supplemented 2mM GlutaMAX, 100U/mL

penicillin, 100ug/mL of streptomycin, and 0.3% bovine serum albumin (BSA) were used as complete growth media. Immediately prior to infection, 5ug/mL or 2.5ug/mL of N-acetylated trypsin (NAT) was added to IM when infecting MDCK or MDCK-SIAT1 cells, respectively.

*PBS and PBS+*

1X phosphate-buffered saline (PBS) was made from 10X stocks with autoclaved MilliQ water. PBS+ was made from 1X PBS supplemented with 100mg/L CaCl<sub>2</sub> and 100mg/L MgCl<sub>2</sub>.

*RT-PCR*

Viral RNA was isolated using Qiagen QIAamp Viral RNA Mini Kit per manufacturer’s protocol. 140ul of nasopharyngeal swab sample was used for each extraction. Concentration of extracted vRNA were measured by NanoDrop and 2ul of vRNA were input into RT-PCR. One-step RT-PCR master mix was prepared with SuperScript™ III One-Step RT-PCR System with Platinum™ Taq DNA Polymerase per manufacturer’s instruction. All 4 primers were added to the mix at final concentration of 10uM. Primer sequences are listed in table 2. Thermocycling protocol was set as: 60°C 1 minute, 42°C 20 minutes, 50°C 20 minutes, 95°C 15 minutes, 35 cycles of 30 seconds at 94°C, 30 seconds at 52°C, 1 minute at 72°C, then 72°C for 10 minutes, finally hold at 12°C. DNA gel was run at 150mV in 1% agarose and TAE buffer.

B/Victoria	Bvf224	ACATACCCTCGGCAAGAGTTTC
	Bvr507	TGCTGTTTTGTTGTTGTCGTTTT
B/Yamagata	BYf226	ACACCTTCTGCGAAAGCTTCA
	BYr613	CATAGAGGTTCTTCATTTGGGTTT

Table 2: Sequences of primers used for lineage identification RT-PCR.

### *MDCK-SIAT1 cell*

Cells were split 1:10 or 1:20 when confluent. 10mL of 1X trypsin-EDTA was used to resuspend cells. CM was added to the flask after each passage. Cells were cultured at 37°C with 5% CO<sub>2</sub>.

### *hNEC cell culture*

Human nasal epithelial cells were obtained from disease-free donors during endoscope sinus surgery from collaborating lab or bought from commercially available source. Cells were differentiated and grown at air-liquid interface (ALI) as previously described [49]. Confluent cultures were trypsinized and plated onto human type IV placental collagen coated 12-well Falcon filter inserts. LHC Basal Medium was added to basolateral side with supplements previously described [49] and cells were cultured at 37°C with 5% CO<sub>2</sub>.

### *Generating virus stocks*

MDCK-SIAT1 cells were seeded in T75 flask and incubated at 37°C with 5% CO<sub>2</sub> until confluent. Cells were washed twice with PBS+, then 2.5mL of virus in IM was added at an MOI = 0.01 infectious units per cell, assuming  $1.125 \times 10^7$  cells/T75 flask. Rock the flask at room temperature for 1 hour. Virus inoculum was aspirated out and cells were washed once again with PBS+. 12mL of IM was added to the flask. Cells were incubated at 32°C and observed every day. Media was collected in a conical tube when 70% of cytopathic effect was seen. The tube was centrifuged at 400g for 10 minutes at 8°C to remove cell debris. The supernatant was



aliquoted into 500ul and stored at -75°C.

#### *Fifty percent tissue culture infectious dose (TCID<sub>50</sub>)*

MDCK-SIAT1 cells were seeded in 96-well plates and incubated at 37°C with 5% CO<sub>2</sub> until confluent. Cells were then washed with 100ul of PBS+ per well twice, and 180ul of IM was added to each well. Virus samples were serially diluted 8 times in a U-bottom 96 well plate with each 1:10 dilution consisting of 180ul of IM and 20ul of the original virus sample or the previous dilution. 20ul of each dilution was pipetted to the appropriate wells in the 96-well plate with cells. The plates were incubated at 32°C with 5% CO<sub>2</sub> for 6 days. Then cells were fixed by adding 80ul of 4% formaldehyde to each well and incubating overnight at room temperature. The media/fixative was removed and 80ul of naphthol blue-black dye was added to each well overnight. Plates were washed with water the next day and TCID<sub>50</sub> titer was quantified.

#### *Flow cytometry*

MDCK-SIAT1 cells were plated at about 50% confluency in 6-well tissue culture plates and incubated at 37°C for 24 hours. Cells were washed twice with PBS+ and then infected with 250ul of virus at MOI = 0.2 and incubated at 32°C. At 18 hours post infection, cells were washed twice with PBS and treated with 1X trypsin-EDTA solution for 15 minutes at 37°C. Dislodged cells were collected in a 50mL conical tube and equal volume of complete growth media was added to the tube. The tube was centrifuged at 800g for 4 minutes, followed by 2 washes with 10mL of PBS. One mL of 2% paraformaldehyde was added to each tube and incubated at 4°C for

30 minutes, followed by 2 washes with 10mL of PBS and centrifuged at 900g for 3 minutes. The fixed cells were permeabilized with 1mL of permeabilization buffer (0.2% of Tween-20 in PBS) at 4°C for 15 minutes. Cell were resuspended in FACS buffer (0.3% BSA in PBS) and aliquoted into FACS tubes. 100uL of blocking buffer (1% normal goat serum in FACS buffer) was added to FACS tubes and incubated at room temperature for 30 minutes. Then cells were washed and centrifuged with 2mL of FACS buffer and incubated with the appropriate 100uL primary antibody for 45 minutes at room temperature. B/Victoria specific mouse monoclonal antibody BR7B7 was used at 4ng/ml, and B/Yamagata specific mouse monoclonal antibody WI3E8 was used at 1ng/ml. Cells were washed twice with 2mL of FACS buffer and incubated with 100uL secondary Goat anti-mouse IgG AF488 at 2ng/ml for 25 minutes at room temperature. Cells were washed with 2mL and resuspended in 500uL of FACS buffer. Ran samples on BD FACSCaliber.

## Results

### *Lineage identification of IBV clinical samples by RT-PCR*

IBV-positive nasopharyngeal (NP) swab samples collected from patients enrolled in the Johns Hopkins Hospital Emergency Room were subjected to viral RNA extraction. The 2017-18 season was a B/Yamagata dominated season in terms of IBV cases (Figure 1.2) [35]. Almost all NP swab samples from that season were B/Yamagata positive (Figure 2.1) or did not generate a band due to low virus titers. Some samples generated double or multiple bands which may be the result of overamplification, or due to the existence of some host materials in NP swab. Notably, sample 11-Pro-365 had double bands and each band were at approximately similar in length to

the 2 expected products at 284bps and 388bps. I suspected that it was a co-infection with both IBV lineages, and a plaque purification was attempted to isolate the B/Victoria clinical strain. All picked plaques still had the double bands at similar sizes as before, and only the gel image of 2 representative plaques was shown (Figure 2.2). Eventually we decided to switch to the 2016-17 influenza season to isolate B/Victoria viruses as it was only one season prior and less B/Yamagata-dominated. Similar procedures were carried out for 2016-17 season NP swab samples, and we were able to identify multiple B/Victoria-positive clinical strains (Figure 2.3).

#### *Passage of IBV clinical strains on hNEC culture and growing virus stocks*

A total of 4 samples (11-Pro-250, 11-Pro-300, 11-Pro-0001, 11-Pro-0122) were selected to be used as the clinical strains in my thesis research. The NP swab samples were inoculated onto the apical side of hNEC culture and incubated at 32°C. Virus production was quantified from apical washes collected at day 3, 5 and 7 post infection and infectious particle titers were measured using TCID<sub>50</sub> assay. All 4 strains showed positive replication and infectious virus production in hNEC cultures. The harvested apical media were then used to grow virus working stocks using MDCK-SIAT1 cells at 32°C. IBV lineages of the new stocks were confirmed again using similar procedures by RT-PCR, and all viruses had the same lineages as their original NP swab samples.

#### *Flow cytometry to validate the lineages of IBV clinical strains*

A protocol using flow cytometry was developed to re-confirm the lineage of our IBV clinical strain working stocks, and to have an alternative method for IBV lineage identification.

When MDCK-SIAT1 cells were infected with B/Baltimore/R0001/2016, a B/Victoria virus, the B/Victoria-specific mouse monoclonal antibody was able to recognize the HA on the surface of infected cells (Figure 4A, B), while experiencing low to no recognition of HA on cells infected by B/Baltimore/R0250/2018, a B/Yamagata virus (Figure 2.4E, F). When a B/Yamagata-specific mouse monoclonal antibody was used, it recognized B/Yamagata virus infected cells well but did not react with B/Victoria infected cells (Figure 4C, D, G, H). Their lineages were also triple confirmed by sequencing the HA segments (see Chapter 4). Hence, we were confident that we now have obtained 2 clinical isolates from each IBV lineage.

## Discussion

IBV lineage identification by RT-PCR is a standard test by WHO for differentiating between B/Victoria and B/Yamagata lineages. We have shown that the recommended protocol and primers sets work well with 2016-17 and 2017-18 flu season IBV clinical isolates. We were able to identify the lineages of our IBV clinical strains and isolate the viruses. Flow cytometry was also shown to be a good tool for IBV lineage differentiation. Although it is not as easy or fast to run, we have demonstrated that it can be a useful alternative method or as a validation for the RT-PCR assay.

It was ideal to have clinical strains of both lineages from the same year for the proposed thesis research. Although we did get a few B/Victoria positive samples after scanning more than 70 NP swabs from the 2017-18 season, they did not show positive replication of infectious virus in hNEC culture and had very weak bands for the B/Victoria specific RT-PCR reaction, indicating low viral load in the swab samples. RT-PCR is a very sensitive test, it is also possible

that the samples had no infectious viruses but did have residual viral RNA which caused the assay to be positive. Given that it was a B/Yamagata-dominated season in IBV, we had to go back to the previous influenza season to try to identify replication-positive B/Victoria clinical strains. The B/Victoria component of the WHO-recommended composition of influenza virus vaccines for 2017-18 did not change from the 2016-17 composition [50, 51]. WHO reported that the majority of B/Victoria circulating strains of the 2016-17 and 2017-18 seasons were well inhibited by antisera from ferrets infected by B/Brisbane/60/2008, the B/Victoria component in flu vaccines for both seasons [50, 51]. Both flu seasons also experienced low percentage of B/Victoria cases, meaning that the virus used as the B/Victoria component was a good match to the majority of circulating strains, and there was probably no major difference between B/Victoria circulating strains from the two seasons. However, it is worth noting that a substantial portion of more recent viruses from 2017-18 season showed poor inhibition by these antisera, while well inhibited by B/Colorado/06/2017-infected antisera. These viruses had a 2-amino acid deletion in HA at residues 162 and 163 [52].

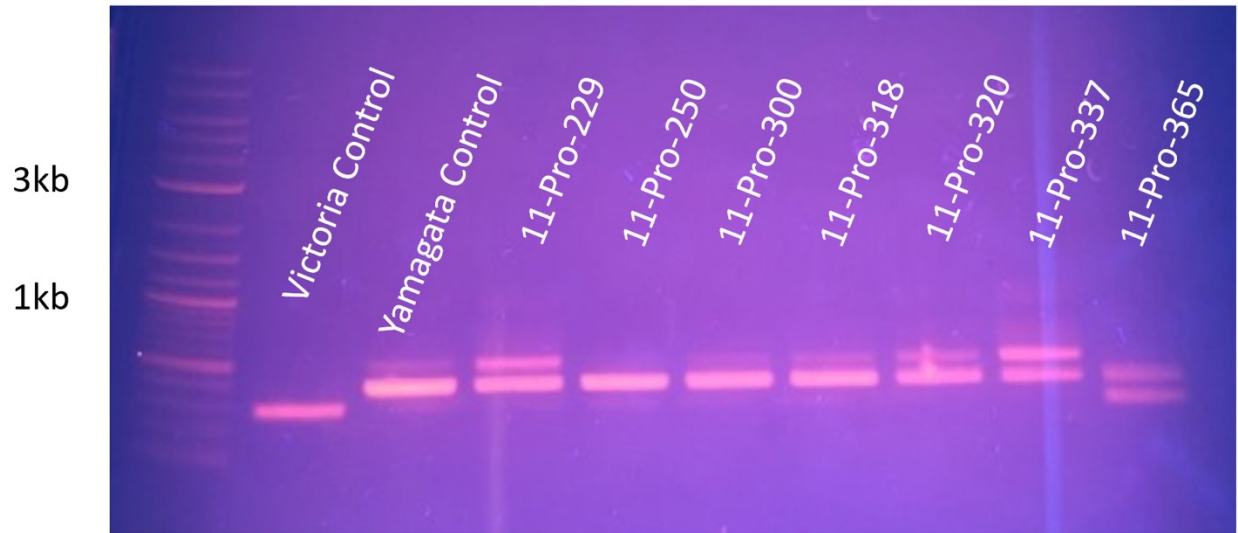


**Figure 2.1: Gel image of RT-PCR products of IBV-positive NP swab samples from the 2017-18 flu season.** Samples were labeled by their patient IDs. More samples were screened and only n=7 representative samples were shown in the image. B/Brisbane/60/2008 and B/Wisconsin/01/2010 were used as B/Victoria and B/Yamagata controls, respectively.

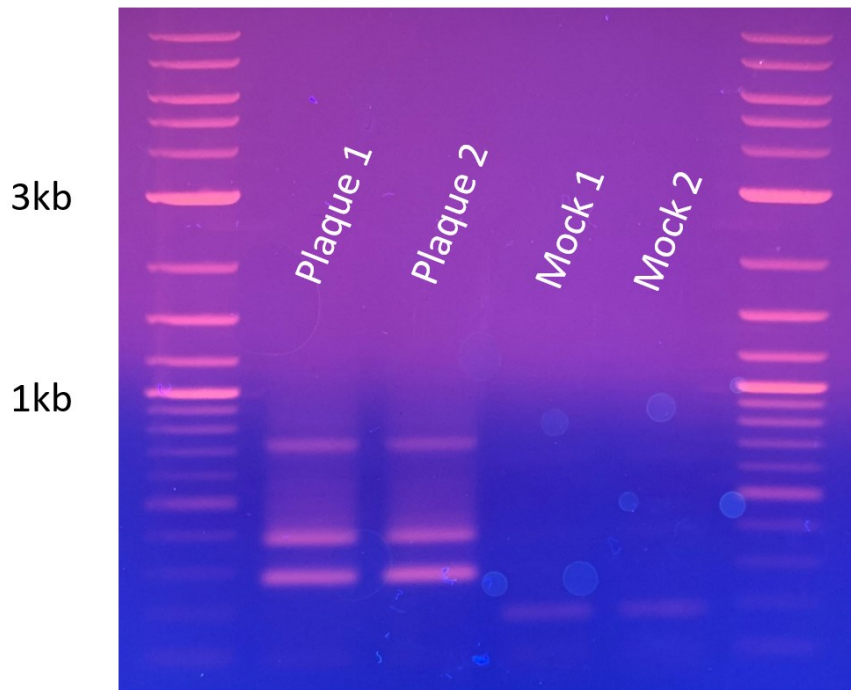


**Figure 2.2: Gel image of RT-PCR products of isolated plaques from plaque purification of NP swab sample 11-Pro-365.** A total of n=10 non-overlapping plaques were picked and screened, only n=2 representative plaques were shown in the image.

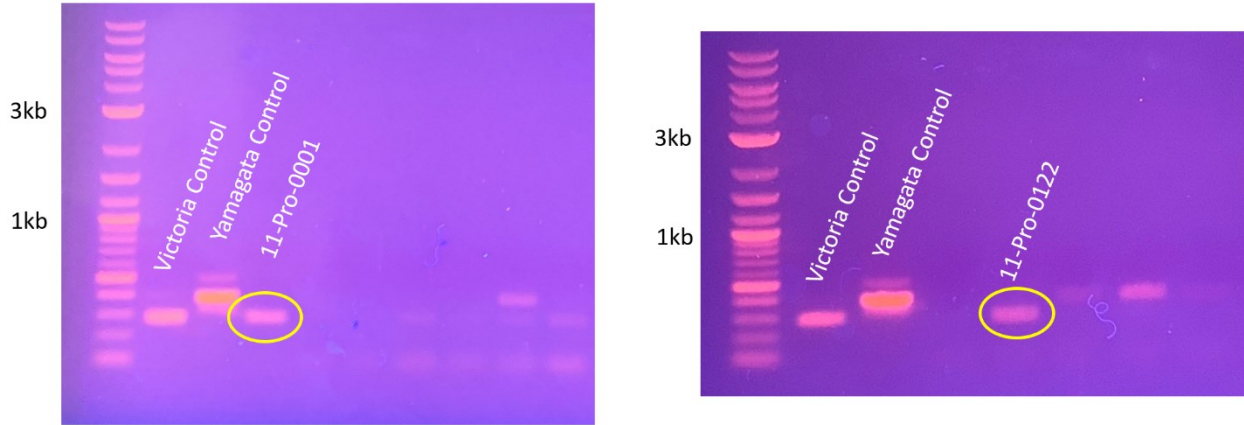


**Figure 2.3: Gel image of RT-PCR products of IBV-positive NP swab samples from the 2016-17 flu season.** B/Brisbane/60/2008 and B/Wisconsin/01/2010 were used as B/Victoria and B/Yamagata controls, respectively.

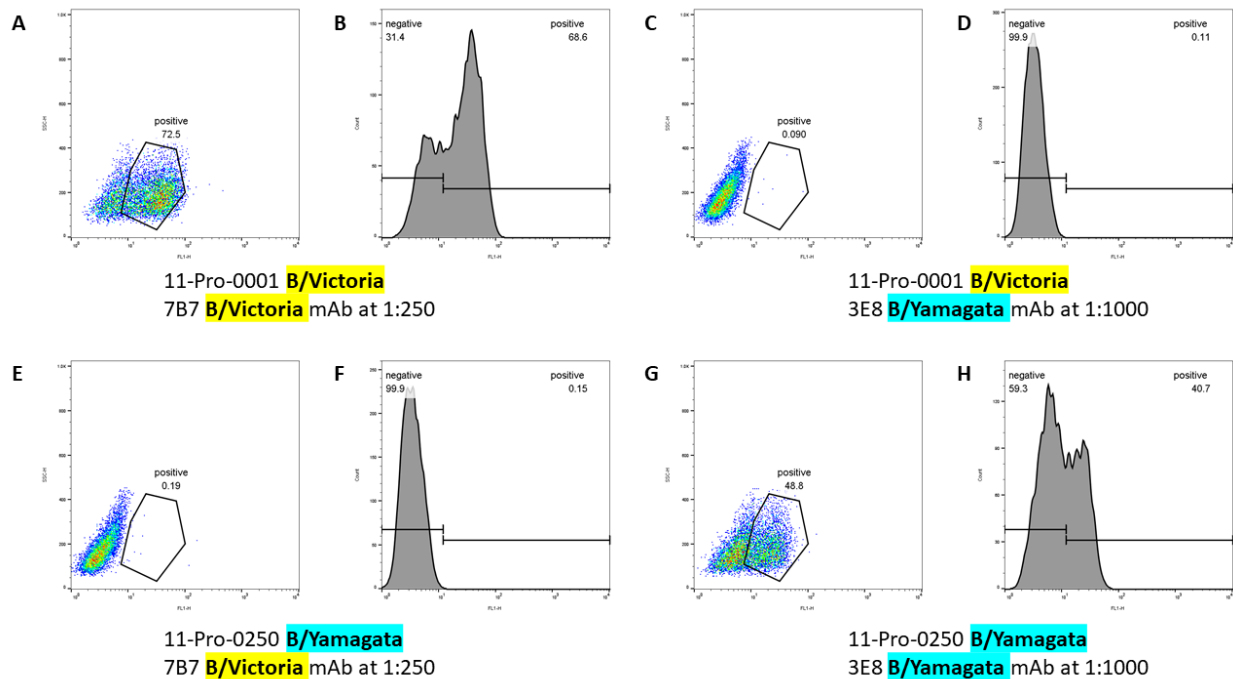


**Figure 2.4: Flow cytometry for IBV clinical strain lineage identification.** Scatter plots and histograms were shown for each virus and antibody pair: **A.** and **B.** B/Victoria virus and B/Victoria-specific antibody, **C.** and **D.** B/Victoria virus and B/Yamagata-specific antibody, **E.** and **F.** B/Yamagata virus and B/Victoria-specific antibody, **G.** and **H.** B/Yamagata virus and B/Yamagata-specific antibody. Mock infected cells with no primary antibody were used for gating. Negative controls were set to be between  $10^0 - 10^1$  on the X axis. Analysis was done on FlowJo.

## **Chapter 3. Viral phenotype characterization of egg-adapted, cell-adapted vaccine strains and circulating strains from both lineages**

### **Rationale**

Basic characterization of our IBV strains involves 2 main experiments: plaque assays and low MOI growth curves. They can provide qualitative comparison of replication fitness between strains. The three comparison groups to be investigated are: i) B/Yamagata circulating strains vs B/Victoria circulating strain, ii) circulating strain vs egg-derived vaccine strain vs cell-derived vaccine strain in B/Victoria, and iii) circulating strain vs egg-derived vaccine strain vs cell-derived vaccine strain in B/Yamagata.

Plaque morphology is an indication for viral fitness. The monolayer of cells is covered by an agarose overlay which prevent viruses from diffusing freely into the media to infect cells that are distal to the initially infected cells. This assay can quantify how viruses infect neighboring cells or spread cell to cell. Faster replicating strains can spread to adjacent cells faster and produce bigger plaques. Plaques are areas of dead cells which cannot be stained with our live cell dyes. If a virus can generate a higher CPE, the plaques will be clearer. MDCK cells were used for plaque assays instead of MDCK-SIAT1 because SIAT1 cells were not able to adhere to the tissue culture dishes strongly enough under assay conditions.

Low MOI growth curves tell us about the replication kinetics of the virus. A virus is said to be more fit when it can produce infectious viruses faster, and/or to a higher peak titer. If the inoculation dose is within 5-fold of each other, any difference in virus titer we see in later time



points can be considered due to intrinsic characteristics of the viruses tested. Growth curves in this chapter were done in 2 cell culture systems. MDCK-SIAT1 cells are a commonly used transformed cell line for influenza virus. hNEC cultures represent the cell type IBV naturally infects and are primary, differentiated cultures. The results generated from hNEC cultures are more biologically relevant to the real world.

## Materials and Methods

### *MDCK-SIAT1 cell*

Cells were split 1:10 or 1:20 when confluent. 10mL of 1X trypsin-EDTA was used to resuspend cells. CM was added to the flask after each passage. Cells were cultured at 37°C with 5% CO<sub>2</sub>.

### *hNEC cell culture*

Human nasal epithelial cells were obtained from disease-free donors during endoscope sinus surgery from collaborating lab or bought from commercially available source. Cells were differentiated and grown at air-liquid interface (ALI) as previously described [49]. Confluent cultures were trypsinized and plated onto human type IV placental collagen coated 12-well Falcon filter inserts. LHC Basal Medium was added to basolateral side with supplements previously described [49] and cells were cultured at 37°C with 5% CO<sub>2</sub>.

### *Plaque assay*

MDCK cells were seeded in 6-well plates to be confluent on day 3. Extra cells were seeded to make sure the plate is fully confluent by the day of the assay. On day 3, cells were washed twice with PBS+. Virus dilution was done on a separate 24-well plate. 900ul of IM was added to 6 wells per virus on the dilution plate. 100ul of virus sample was added to the first well. 1:10 serial dilution was done on each sample until  $10^{-6}$ . Then 250ul of the virus dilution was added directly to the appropriate wells on the 6-well plate. Plates were incubated at 32°C for 1 hour and shaken every 10-15 minutes to ensure even distribution of inoculum. After 1 hour, virus was aspirated out and 2% agarose was mixed with 2X plaque media (2X modified eagle medium supplemented with 2mM GlutaMAX, 100U/mL penicillin, 100ug/mL streptomycin, 0.3% BSA, 5mM HEPES buffer, and 5ug/mL N-acetyl trypsin) and 2mL of the resulting 1% agarose was overlaid to each well. Plates were then put in 32°C incubator after agarose had solidified. Plates were observed every day and fixed overnight with 4% formaldehyde when plaque reached desired sizes. The agarose overlay was scooped out the next day, and cells were stained with naphthol blue-black. Plaques were imaged by light dissection microscope. Plaque size was quantified by Image J. Area under the hand-drawn shape tracing the edge of plaque was measured. Overlapping plaques were not sampled.

### *MDCK-SIAT1 growth curve*

Cells were seeded in 24 well plates to be confluent on day 2. On the day of infection, cells were washed twice with PBS+. Virus dilution to an MOI of 0.001 was prepared, assuming  $3 \times 10^5$  cells/well. 100ul of virus dilution was added to 3 wells per virus. The plate was rocked for

1 hour at room temperature. Then virus inoculum was aspirated, and cells were washed twice with PBS+. Five hundred ul of IM was added back to each well and incubated at 32°C. Infected cell supernatants were collected and replaced with fresh IM at 2, 12, 24, 36, 48, 72 and 96 hours after infection. Collected timepoint samples were stored at -75°C. Infectious virus titers in those samples were measured with TCID<sub>50</sub> assay.

#### *hNEC growth curve*

300ul of warm PBS+ was added to apical side to wash cells twice and basolateral media was replaced. Virus was diluted to an MOI of 0.01, assuming  $3.3 \times 10^5$  cells/well. 100ul of virus inoculum was added to the apical side and cells were incubated at 32°C for 2 hours. Virus was then aspirated out and cells were put back in the incubator. At timepoint 2, 12, 24, 36, 48, 72 and 96 hours after infection, 100ul of IM was added to apical side and incubated in 32°C for 10 minutes. Then media was collected and stored at -75°C. Basolateral media was changed every 2 days. Infectious virus titers in the apical supernatants were measured with TCID<sub>50</sub> assay.

#### *Fifty percent tissue culture infectious dose (TCID<sub>50</sub>)*

MDCK-SIAT1 cells were seeded in 96-well plates and incubated at 37°C with 5% CO<sub>2</sub> until confluent. Cells were then washed with 100ul of PBS+ per well twice, and 180ul of IM was added to each well. Virus samples were serially diluted in a U-bottom 96 well plate. Each 1:10 dilution consisted of 180ul of IM and 20ul of the original virus sample or the previous dilution. Each sample was diluted 8 times to 10<sup>-8</sup>. 20ul of each dilution was pipetted to the appropriate

wells in the 96-well plate with cells. The plates were incubated at 32°C with 5% CO<sub>2</sub> for 6 days. Then cells were fixed by adding 80ul of 4% formaldehyde to each well and incubating over night at room temperature. The media/fixative was removed and 80ul of naphthol blue-black dye was added to each well over night. Plates were washed with water the next day and TCID<sub>50</sub> titer was quantified.

## Results

### *Plaque morphology*

Plaque assay was performed on MDCK cells at 32°C. When comparing across lineages, both B/Yamagata clinical strains had larger plaque sizes compare to B/Victoria clinical strains. The B/Yamagata mean plaque size was  $3.43 \pm 1.27 \text{ mm}^2$  for B/Baltimore/R0250/2018 and  $3.10 \pm 1.56 \text{ mm}^2$  for B/Baltimore/R0300/2018 (Figure 3.1 A). The B/Victoria mean plaque size was  $1.56 \pm 0.89 \text{ mm}^2$  for B/Baltimore/R0001/2016 and  $1.07 \pm 0.54 \text{ mm}^2$  for B/Baltimore/R0122/2016 (Figure 3.1 A). There was no major difference in plaque clarity both between strains within a lineage and across lineages. Plaques were transparent and viruses were able to clear the monolayer of cells well (Figure 3.1 B-E).

Plaque comparison within a lineage was also done on clinical strains, egg-derived vaccine strains and cell-derived vaccine strains. In the B/Yamagata lineage, the mean plaque sizes for B/Baltimore/R0250/2018, B/Phuket/3073/2013 egg-derived and B/Phuket/3073/2013 cell-derived were  $1.03 \pm 0.64 \text{ mm}^2$ ,  $1.16 \pm 0.50 \text{ mm}^2$  and  $0.76 \pm 0.42 \text{ mm}^2$ , respectively (Figure 3.1 F). The B/Baltimore/R0250/2018 plaques had different sizes compared to the previous assay because they were done as separate experiments. No significant difference in plaque size was

observed between the circulating strain and the egg-derived vaccine strain, while the cell-derived vaccine strain had larger mean plaque sizes when compared to both egg-derived vaccine strain and circulating strain. Plaque clarity was similar across the 3 virus strains. Most plaques were not clear and were stained light blue in the center (Figure 3.1 G-I).

In the B/Victoria lineage, the mean plaque sizes for B/Baltimore/R0001/2016, B/Colorado/06/2017 egg-derived and B/Iowa/06/2017 cell-derived were  $0.59 \pm 0.40 \text{ mm}^2$ ,  $0.60 \pm 0.37 \text{ mm}^2$  and  $0.39 \pm 0.25 \text{ mm}^2$ , respectively (Figure 3.1 J). The cell-derived vaccine strain had smaller plaques than both other strains. Plaque clarity was similar across the three strains. Most plaques were not clear and were stained light blue in the center (Figure 3.1 K-M).

#### *Low MOI growth curve*

To compare replication fitness between the two lineages, a low MOI growth curve was done on the four circulating strains at 32°C. No significant fitness advantage was observed among the strains tested in both MDCK-SIAT1 and hNEC cultures (Figure 3.2 A, B). Peak titer was reached at 48 hours post infection, and viral replication rate was similar across all strains.

The comparison between the circulating strain and two vaccine strains of B/Yamagata lineage revealed that cell-derived vaccine strains replicated more slowly than the other two strains and reached a lower peak titer (Figure 3.2 C, D). In MDCK-SIAT1 cell culture, B/Phuket/3073/2013 cell-derived virus reached peak titer at 36 hours post infection, while B/Baltimore/R0250/2018 and B/Phuket/3073/2013 egg-derived virus reached peak titer at 48 hours post infection and at 1.9 and 1.3 log higher level, respectively (Figure 3.2 C). Infectious virus titer started to drop after 48 hours post infection due to cell death. A similar trend was

observed in hNEC cultures (Figure 3.2 D). All strains reached peak titers between 36 and 48 hours post infection, but the cell-derived vaccine strain had peak titer more than 2 logs below the other two strains. Infectious virus titer reached a plateau and remained steady around their corresponding peak titer after 48 hours. No significant difference in viral replication fitness was detected between the circulating strain and the two vaccine strains from the B/Victoria lineage (Figure 3.2 E, F). All strains reached peak titer between 48 and 72 hours post infection in both MDCK-SIAT1 and hNEC cultures. In all growth curves, hNEC culture consistently produce 1 to 2  $\log_{10}$  higher peak titers than MDCK-SIAT1 culture.

## Discussion

The plaque assays were repeated twice for each comparison to ensure reproducibility. Since the end point of a plaque assay is subjective, data could not be compared across different experiments. Although plaque size bear similar trends between assays, we noticed that plaque morphology was not very consistent. Sometimes the plaque was clear, the next assay with the same virus may produce semi-clear plaques. The cells themselves could contribute to the inconsistency of plaque morphology. Since there was no way to accurately quantify the confluency of cells, the monolayer could be in slightly different confluency in every assay. Cell passage number could also affect condition of the cells.

The two B/Yamagata circulating strains consistently produce larger plaques than the two B/Victoria circulating strains in plaque assay (Figure 3.1 A). However, low MOI growth curves in both hNEC and MDCK-SIAT1 cultures suggest no difference between the four strains in replication kinetics (Figure 3.2 A, B). This result suggests that there may be differences between

lineages in the ability for virus to spread cell-to-cell, but the advantage B/Yamagata had may be masked when virus progenies can diffuse freely in media and infect distal cells. A recent study in IAV showed that IAV can spread to adjacent cells via tunneling nanotubes [53]. The group showed that HA deficient IAV could transport its viral genome to recipient cells. Productive infection was also observed in those cells. At the time of writing, no similar phenomenon has been reported in IBV.

In the first several B/Victoria growth curves, virus inoculums had larger than 5-fold differences from each other, meaning any differences we saw in later timepoints may not be due to viral characteristics alone. The original stock was measured multiple times to reconfirm its infectious virus titer. Eventually, we pre-made virus serial dilutions separated by 5-fold each and tittered these dilutions. Then picked the samples with similar TCID<sub>50</sub> titers to do the growth curve. Each growth curve was repeated twice to confirm the trend.

In both B/Yamagata and B/Victoria lineages, the cell-derived vaccine strains had smaller plaques, suggesting possible changes to the virus by cell-adaptation. Those changes could be on HA or internal proteins such as the PA, PB1 and PB2 polymerase complex. The lower viral fitness of the cell-derived B/Yamagata vaccine strain in both MDCK-SIAT1 and hNEC growth curves reconfirmed the finding in plaque assays. Interestingly, while we observed a fitness cost in plaque assays of both cell-derived vaccine viruses (Figure 3.1 F, J), a slower replication phenotype was only captured in B/Yamagata cell-derived virus by growth curves (Figure 3.2 C, D). This may also be a result of differential ability of cell-to-cell spread between lineages. B/Victoria viruses may depend more on virus budding to spread, and cell-adaptation only caused reduction in ability of viruses to spread to adjacent cells. Overall, the data supports that cell-derived vaccine viruses may induce phenotypes with slower replication in both *in vitro* cell lines

and primary cell cultures.



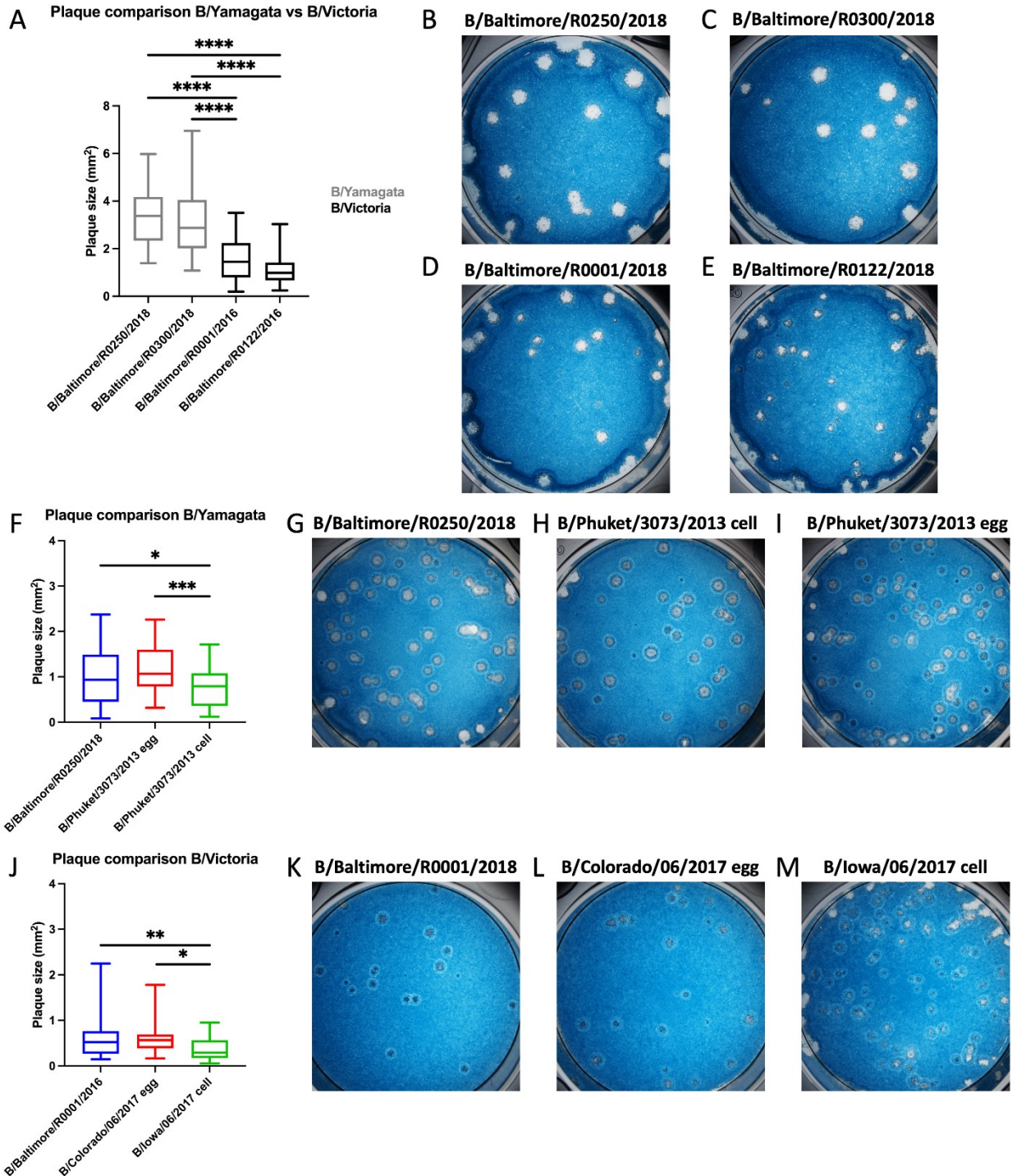


**Figure 3.1: Plaque Assays.** **A.** Comparison of plaque sizes formed by circulating strains of both lineages. **B-E.** Representative images of plaques from each strain. **F.** Comparison of plaque sizes formed by B/Yamagata IBV strains. **G-I.** Representative images of plaques from each strain. **J.** Comparison of plaque sizes formed by B/Yamagata IBV strains. **K-M.** Representative images of plaques from each strain. Asterisks denote statistically significant differences ( $* = p < 0.05$ ) via one-way ANOVA with multiple comparisons.

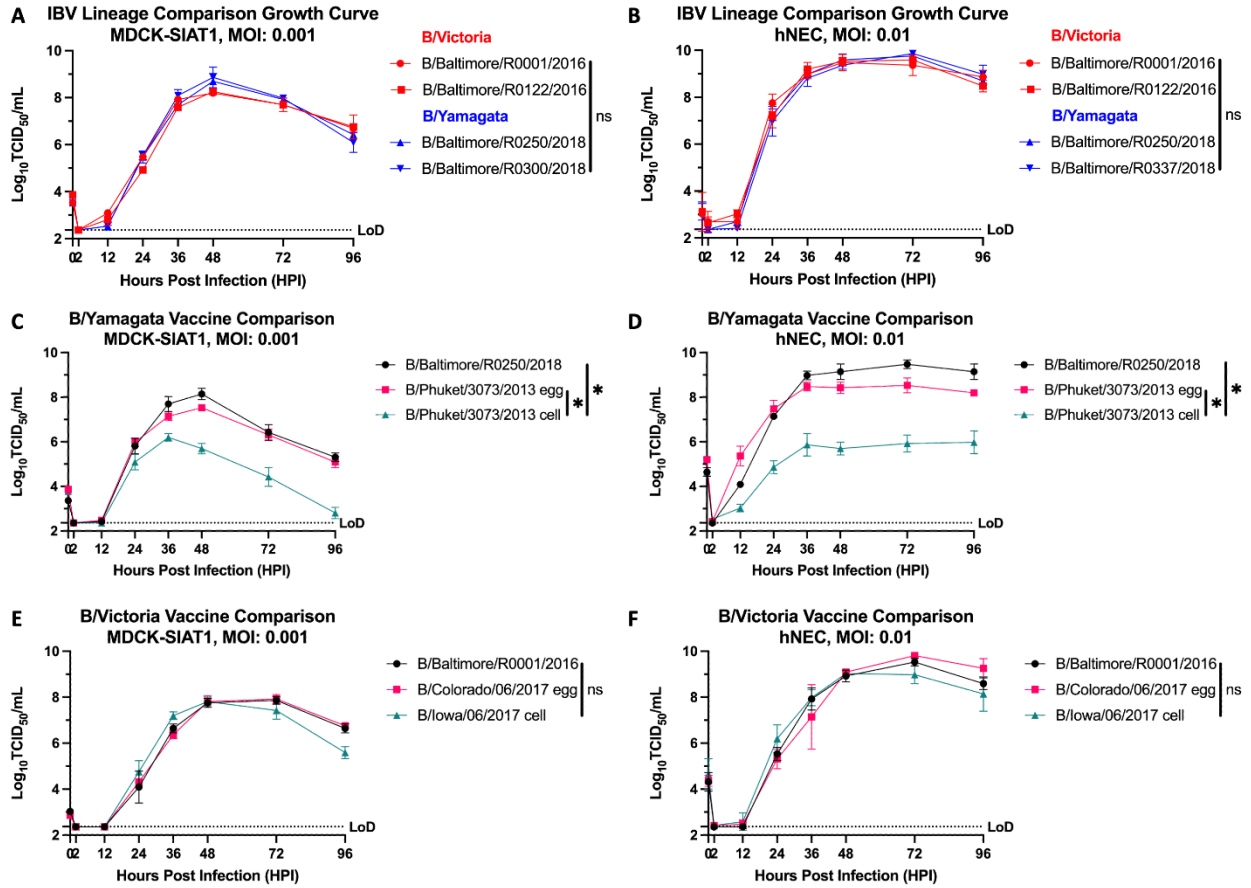


**Figure 3.2: Low MOI Growth Curves.** **A.** Low MOI growth curve of all circulating strains of both lineages on MDCK-SIAT1 culture and **B.** hNEC culture. **C.** Low MOI B/Yamagata growth curve of circulating strain, egg-derived and cell-derived vaccine strains on MDCK-SIAT1 culture and **D.** hNEC culture. **E.** Low MOI B/Victoria growth curve of circulating strain, egg-derived and cell-derived vaccine strains on MDCK-SIAT1 culture and **F.** hNEC culture. Asterisks denote statistically significant differences ( $* = p < 0.05$ ) by repeated measures MANOVA with Tukey multiple comparison tests.

## **Chapter 4. Sequencing of HA segment and differential neutralizing antibody titers against vaccine and circulating strains**

### **Rationale**

In the previous chapter we demonstrated that there are phenotypic differences between vaccine and circulating virus strains in both IBV lineages. Although multiple factors may contribute to the differences, we sought to investigate if there are changes in the HA sequences of these viruses which could potentially explain the different phenotypes. We chose the HA segment because it is one of the main antigens of which humans mount an antibody response to. Changes in HA can impact vaccine efficacy and cause viral fitness change [25, 32, 44, 54].

As discussed in earlier chapters, IBV egg adaptation was well documented [42, 43, 55]. It was reported that the percentage of egg-propagated viruses that were antigenically similar to the circulating strains was significantly lower when compared to cell-propagated viruses from 2008 to 2018 [55]. The greater discrepancy was seen in B/Victoria lineages. As a final analysis, I wanted to determine if egg or cell propagation induced changes in the HA protein sequence of our IBV strains.

### **Materials and Methods**

#### *RT-PCR*

Viral RNA was isolated using Qiagen QIAamp Viral RNA Mini Kit per manufacturer's

protocol. 140ul of virus stock was used for each extraction. The concentration of extracted vRNA were measured by NanoDrop and 2ul of vRNA were input into the RT-PCR reaction. One-step RT-PCR master mix was prepared with SuperScript™ III One-Step RT-PCR System with Platinum™ Taq DNA Polymerase per manufacturer's instruction. The PCR primers were added to the mix at final concentration of 10uM. Primer sequences are listed in Table 3. Thermocycling protocol was set as: 60°C 1 minute, 42°C 20 minutes, 50°C 20 minutes, 95°C 15 minutes, 35 cycles of 30 seconds at 94°C, 30 seconds at 52°C, 1 minute at 72°C, then 72°C for 10 minutes, finally hold at 12°C. DNA gel was run at 150mV in 1% agarose.

B/Yamagata RT-PCR primer	IBV_Yam_5UTR_1F	AGCAGAAGCAGAGCATTTTCT
	IBV_Yam_3UTR_1842R	TGATGACAAGCAAACAAGCACT
B/Victoria RT-PCR primer	IBV HA 5' UTR	TATTCGTCTCAGGGAGCAGAAGCAGAGCATTTTCT
	IBV HA 3' UTR R	GTAATGATGACAAGCAAACAAGCA
Sequencing primer	IBV HA seq 426 F	AGAAAAAGCACGACCAGGAGGACCCTA
	IBV HA seq 1316 R	AGTATTTTCGTTGTGGAGTTCATCCAT

Table 3: Sequences of PR-PCR primers and sequencing primers for IBV HA sequencing.

### *Sequencing*

After cDNA generation, the product was purified using QIAquick PCR Purification Kit per manufacturer's protocol. Final concentration of cDNA was quantified using NanoDrop. The cDNA was sent to the Synthesis & Sequencing Facility of the Johns Hopkins University for Sanger sequencing. The 2 PCR primers and 2 sequencing primers at 7mM each were included in the tube.

### *HA modeling*

Sequences were retrieved and analyzed using Geneious 8 software. B/Brisbane/06/2008 was used for the IBV HA numbering and the HA crystal structure was used for modeling. HA

modeling was done using Pymol.

## Results

### *RT-PCR of HA segment*

A set of forward and reverse primers were designed for each IBV lineage for RT-PCR of the HA segment. Another pair of sequencing primers which hybridized more to the center of the segment were also used to generate overlapping reads with the outer primers for more sequencing coverage. Initially a universal pair of primers were used since the 3' and 5' ends of the HA segment had similar sequences for both lineages. However, RT-PCR only worked for our B/Victoria viruses, and new pair primers needed to be designed specifically for B/Yamagata. The length of cDNA product was around 1800 bps for all viruses - the expected length of the HA segment in IBV.

### *Amino acid changes and mapping mutations on HA model*

A list of all amino acid mutations for each lineage can be found in the following tables (Table 2, 3). All mutations are named as changes from the circulating strain of the corresponding lineage. There were more nucleotide changes in B/Yamagata lineage but most of them were silent mutations and did not result in amino acid changes in the HA protein. Mutation Q173L, N197D and N230D were on the surface of HA, and V252M was a mutation that was not solvent exposed, so it was not mapped on the HA model. Residue numbers 172 and 197 are close to known antigenic structures called the 120 loop and 190 helix, respectively (Figure 4.1 A).

Residue 197 is a known glycosylation site and the mutation in B/Phuket/3073/2013 egg-derived virus caused the loss of this glycosylation site.

In the B/Victoria lineage, all amino acid changes were on the surface of HA (Figure 4.1 B). Mutation R495K was located at the bottom of the HA stem. Mutation D129G was in the 120 loop and I180V was next to this antigenic site. The egg-derived vaccine strain also possessed a mutation at residue 197, which caused the loss of the glycosylation site. In loop 160, both vaccine strains had two amino acid deletions at residues 162 and 163. Apart from R495K, all mutations in both lineages were located near known antigenic structures.

Amino acid position	B/Baltimore/R0001/2016	B/Colorado/06/2017 egg	B/Iowa/06/2017 cell
129	Asp (D)	Gly (G)	Gly (G)
162, 163	Lys, Asn (K, N)	-	-
180	Ile (I)	Val (V)	Val (V)
197	Asn (N)	Thr (T)	Asn (N)
495	Arg (R)	Lys (K)	Lys (K)

Table 4: All amino acid changes in B/Victoria lineage.

Amino acid position	B/Baltimore/R0250/2018	B/Phuket/3073/2013 egg	B/Phuket/3073/2013 cell
173	Gln (Q)	Leu (L)	Leu (L)
197	Asn (N)	Asp (D)	Asn (N)
230	Asn (N)	Asp (D)	Asp (D)
252	Val (V)	Met (M)	Met (M)

Table 5: All amino acid changes in the B/Yamagata lineage.

### *Differential serum neutralization of egg-derived vaccine virus compared to circulating strain*

To investigate whether the changes we saw in HA affect effective antibody-mediated virus neutralization, Dr. Jo Wilson, the research and clinical fellow in our lab, did neutralization

assay on the B/Yamagata viruses. Baseline and convalescent sera from patients infected with B/Yamagata viruses in the 2017-18 season were collected. The neutralization titers of the sera were measured against B/Baltimore/R0250/2018, B/Phuket/3073/2013 egg-derived virus and B/Phuket/3073/2013 cell-derived virus (Figure 4.2 A). No significant difference was observed in baseline sera titers to the afore mentioned viruses. The convalescent sera had higher neutralization activity to B/Phuket/3073/2013 egg-derived virus than both circulating strain and cell-derived vaccine virus. The 3 high responders in the group were vaccinated individuals.

To further investigate on how egg-adaptation may affect vaccine efficacy, Dr. Wilson also tested the neutralization titers to the B/Yamagata viruses in paired pre- and post-influenza vaccination sera from 67 humans (Figure 4.2 B). All subjects had received quadrivalent vaccine including B/Phuket/3073/2013-like virus prior to the 2019-20 season. Both pre- and post-vaccination sera recognized the B/Phuket/3073/2013 egg-derived virus better than the B/Baltimore/R0250/2018 circulating virus. Post-vaccination serum recognized the B/Phuket/3073/2013 egg-derived virus more effectively than either the cell culture or circulating virus. Taken together, the data indicate that the mutations present in the egg and cell culture vaccine strains of the B/Yamagata lineage viruses affect the antigenic structure of the HA protein, indicating that cell and egg adaption can alter antigenic sites.

## Discussion

We hypothesized that a universal pair of primers would work for RT-PCR of the HA segments for both IBV lineages. We compared several published sequences and found the 3' UTR and 5' UTR of the segment were very similar for both lineages, and the first 30 bases

downstream of the start codon and the last 20 bases upstream of the stop codon were conserved, as well. There could be possible degradation of vRNA at the two ends of the segment which caused the primers not able to bind in the case of our B/Victoria viruses. However, the fact that all 3 of our B/Victoria viruses were able to generate products from their HA segments but none of our B/Yamagata viruses did suggested it may be a systematic problem such as sequence variations. We decided to redesign a new set of primers for B/Yamagata as the process was quick and easy. The new primers bind closer to the starting codon on the 5' end. A few bases downstream of the start codon were not read due to poor sequencing quality of the Sanger Sequencing but since the first 30 bases and 10 amino acids were highly conserved as mentioned above, this did not pose a problem in identifying HA lineages. The first 15 amino acids of the newly translated polypeptide chain will also be cleaved during processing, so even if the sequences were different it would not be problematic.

HA is the surface protein on influenza virus which is responsible for receptor binding and membrane fusion. It is also a common target for antibody binding. Neutralizing antibodies often bind at or near the receptor binding domain on the top of HA. Changes in amino acid residues and glycosylation sites near antigenic sites may alter the binding affinity of neutralizing antibody, causing potential evasion from antibody response in hosts. A mutation at 197 is present in egg-derived vaccine viruses in both lineages, suggesting this may be a common mutation site caused by egg adaptation during vaccine manufacturing. The same mutation in egg-cultured viruses were reported before [43, 44]. Virus with a 197 glycosylation had suppressed replication in eggs, suggesting a disadvantage of this modification for efficient growth in eggs. Glycosylation is also an important factor to the antigenic profile of influenza viruses. If egg adaptation occurred in a vaccine virus, it may not match the antigenic property of the circulating



viruses very well and decrease vaccine efficacy. The result from neutralization assay confirmed our hypothesis in the B/Yamagata lineage. Unfortunately, we could not test the hypothesis in B/Victoria lineage because we were not able to isolate a B/Victoria circulating strain from this year. Further consideration needs to be taken into account when producing egg-based influenza vaccine. Even though the B/Phuket/3073/2013 cell-derived virus had reduced viral fitness, it seemed to preserve similar antigenic properties as the circulating strain. The reduction in replication fitness will not be a setback for inactivated vaccine compared to live attenuated influenza vaccine which requires active viral replication. We also see that cell-derived vaccine strains have fewer mutations on HA compared to egg-derived vaccine strains, especially at key glycosylation sites.

Mutations in HA may also alter the binding affinity to sialic acids, which subsequently increases or decreases infectivity. The decrease in viral fitness of B/Phuket/3073/2013 cell-derived virus in both MDCK-SIAT1 and hNEC cultures may be partly caused by the mutations we found in HA. Viral fitness changes are often associated with mutations on internal proteins, as well. The replicase proteins PA, PB1 and PB2 can also contribute to the rate of influenza virus replication and should also be sequenced to determine if any mutations were acquired during egg and cell adaption.

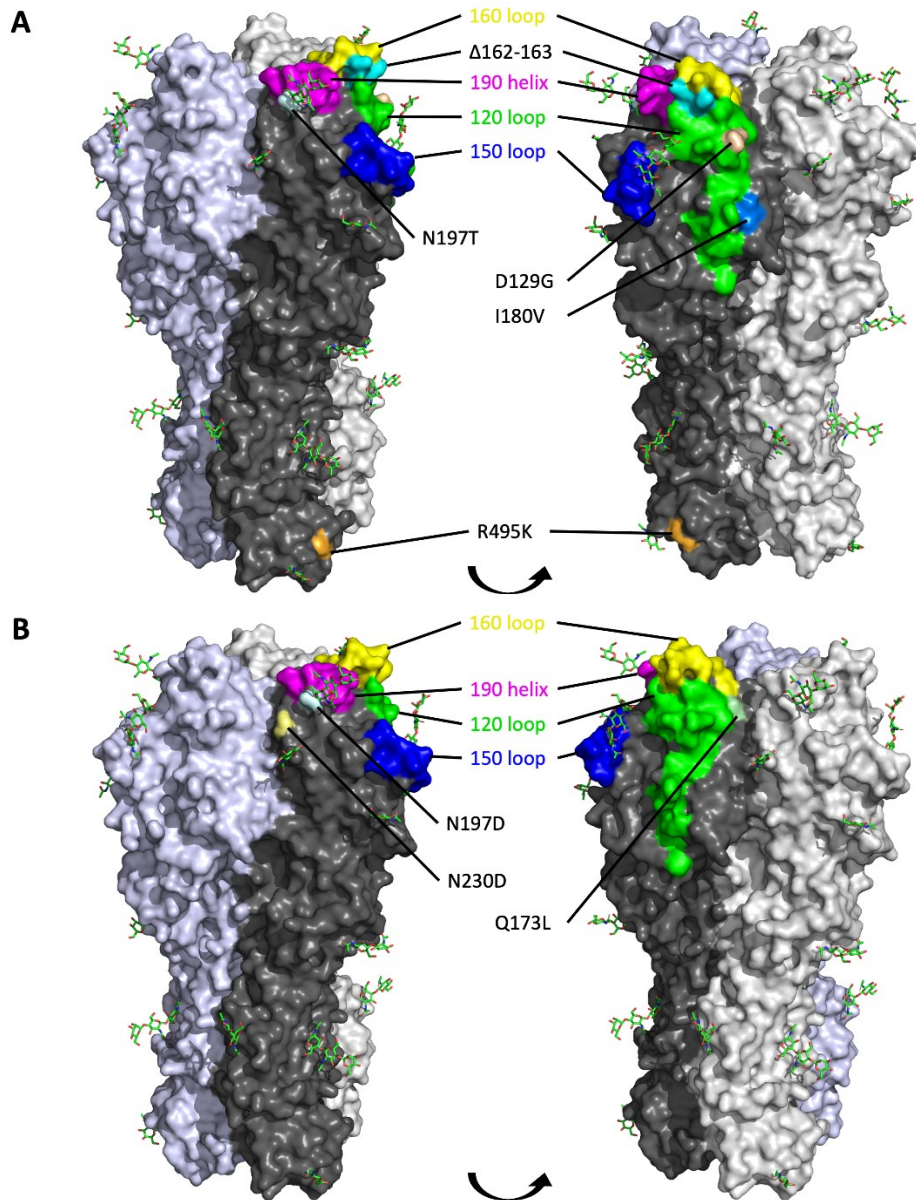


**Figure 4.1: Mutations mapped on IBV HA model.** All mutations on the HA surface of egg-cultured vaccine and cell-cultured vaccine strains from the circulating strain in both **A.** B/Victoria and **B.** B/Yamagata lineages are mapped on the model. A mutation V252M is not shown on the model as the residue is inside the HA trimer structure. The known antigenic sites of IBV are highlighted. The 120 loop is shown in green, the 150 loop is shown in blue, the 160 loop is shown in yellow, and the 190 helix is shown in violet. The crystal structure of HA of B/Brisbane/06/2008 was used for modeling and amino acid numbering.

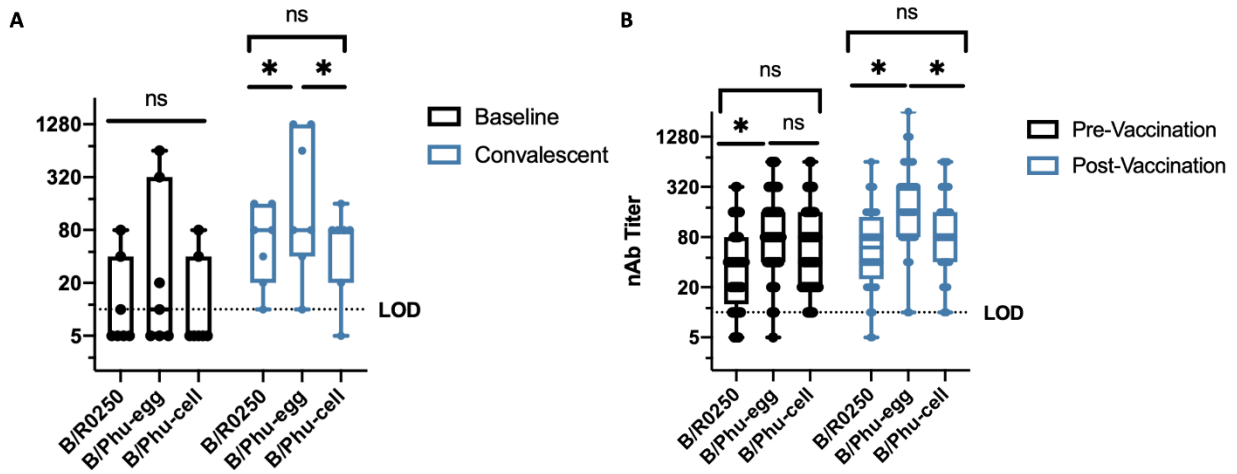


**Figure 4.2: Neutralization assay. A.** Comparison of neutralizing antibody titers using baseline and convalescent sera from B/Yamagata infected patients in 2017-18 season ( $n = 7$ ) and **B.** pre- and post-influenza vaccination in individuals in 2017-18 ( $n = 67$ ). Asterisks denote statistically significant differences ( $* = p < 0.05$ ) via two-way ANOVA with multiple comparisons.

## Chapter 5. Conclusion and Future Direction

In this thesis, I have demonstrated characterization of circulating strains, egg-derived vaccine strains and cell-derived vaccine strains of IBV in both lineages. The whole process started from virus isolation from patient samples to phenotypic characterization, and finally sequencing to try to explain the different phenotypes we observed in these strains. We have shown that B/Victoria and B/Yamagata circulating strains in 2017-18 season had different cell-to-cell spread pattern, but overall replication kinetics are similar. In both lineages, cell-derived vaccine viruses had slower replication in cell cultures, although there seemed to be no antigenic changes to the circulating virus. The sequencing results supported our hypothesis that there were mutations in the HA of cell-derived and egg-derived vaccine viruses. We also proved that these changes on egg-derived vaccine virus led to antigenic changes with our neutralization assay results.

There also are questions we were not able to answer in this thesis. Influenza virus replication kinetics is not only affected by HA. Internal proteins, notably the polymerases and M2 proteins, can also drastically alter replication efficiency. We can also go more in depth on the mutations we found on HA. Specific mutants can be generated with only one of the several mutations and characterized using our workflow to pinpoint mutations that caused the phenotypic change. Sequencing can also be done on the NA protein, as it is also subjected to antigenic drift as mentioned in earlier chapters. A recent PhD graduate from our lab, Dr. Harrison Powell, showed that glycosylation changes on NA in IAV can alter viral fitness and evade antibody binding [56]. A novel genotype of IAV from clade 3c.2a H3N2 encoded

glycosylation site at position 245–247 in the NA protein appeared in 2014-15 season surveillance data. Recombinant virus with 245 NA Gly had lower enzymatic activity and grew to lower virus titer in hNEC cultures compared to virus without the glycosylation. However, this change allowed the virus to evade neutralization by blocking the binding of NA specific antibodies in human sera.

Our data showed reduced virus growth in cell culture adapted viruses and introduction of multiple mutations on HA. However, no change in its antigenic property was captured by the neutralization assay with human sera. These results suggested that cell culture remains to be the better strategy than egg culture in preserving the antigenic sites on IBV HA, thus lowering the risk of vaccine mismatch. However, mutations may still arise and possibly cause lower virus yield in vaccine production.

In the WHO report for vaccine recommendation for the 2020-21 season, a vast majority of B/Victoria viruses tested had a 3 amino acid deletion on HA at positions 162-164 [57]. Ferret antisera raised against the virus with the deletion (B/Washington/02/2019) can effectively neutralize these viruses, but neutralization was poor by ferret antisera raised against strains from previous seasons (B/Colorado/06/2017). This suggests possible antigenic drift of recent B/Victoria viruses. A similar workflow as in this thesis can be implemented to characterize these recent B/Victoria strains. Comparison can be made between older and newer B/Victoria circulating strains as a possible future project.

Similar aspects in IAV have been well studied, but these have not been extensively studied with IBV. Other studies have shown hemagglutinin inhibition assays or ferret antisera neutralization assays, but our data is using human sera neutralization assay. It will be more relevant to influenza surveillance and vaccine work.

## Appendix. SARS-CoV-2 Lung Pathology in Golden Syrian Hamsters

### Background

The coronavirus disease 2019 (COVID-19) started at the end of 2019. The disease is caused by the newly emerged Severe, Acute, Respiratory Syndrome coronavirus 2 (SARS-CoV-2 or SCV2), a betacoronavirus. Multiple publications have indicated a male bias in disease severity and mortality rates [58-61]. To understand the biology of sex differences in COVID-19, a group effort to study SARS-CoV-2 infection in Golden Syrian Hamsters was conducted, and I am very proud to have been part of that team.

Animal models can be used for studying sex differences in the pathogenesis of SCV2. The Golden Syrian Hamster was chosen because they are susceptible to human strains of SVC2 without the need to adapt viruses to generate disease. This study aimed to provide a more thorough analysis of sex differences in the pathology of SCV2 infection, including infectious virus load, viral RNA, cytokines, antibody responses, and lung damage in Golden Syrian Hamster infection model. In this appendix, I will focus on my contribution to the group, which is infectious virus load in tissues. At the point of writing, the manuscript had been submitted to *mBio* for review on 31 March 2021.

### Material and Methods

#### *Tissue homogenization*

Hamster nasal turbinates, lung lobes and tracheal tissue samples, harvested at 2, 4, 7, 14

and 28 days post infection were provided by the animal group. The animals were infected with  $10^5$  TCID<sub>50</sub>s per animal, and the inoculum of 100 ul was divided equally between the two nares. Homogenization media (DMEM with 100 U/mL penicillin and 100 µg/mL streptomycin) was added to each pre-weighed tissue to generate a 10% weight to volume ratio for homogenization. Lysing Matrix D beads were added to each tube and the samples were homogenized in a FastPrep-24 bench top bead beating system (MPBio) for 40sec at 6.0m/s, followed by centrifugation for 5 min at 10,000g at room temperature. Samples were returned to ice and the supernatant was distributed equally into 2 tubes. To inactivate SARS-CoV-2, TritonX100 was added to one of the tubes to a final concentration of 0.5% and incubated at room temperature for 30 minutes. The homogenates were stored at -70C.

#### *TCID<sub>50</sub>*

Infectious virus titers of tissue homogenates were measure by TCID<sub>50</sub> assay. DMEM supplemented with 2.5% fetal bovine serum, 1mM glutamine, 1mM sodium pyruvate, and penicillin (100 U/mL) and streptomycin (100 µg/mL) antibiotics were prepared as infection media for SCV2. Homogenates were serially diluted in IM similarly to the TCID<sub>50</sub> for IBV as described in earlier chapters. Virus dilutions were then transferred to Vero-E6-TMPRSS2 cells seeded in 96-well plates. Cells were incubated at 37°C for 6 days. At the end point, cells were fixed with 4% formaldehyde, and stained with naphthol blue-black. Infectious virus titers were quantified as described for IBV.

## Results

### *Similar SARS-CoV-2 replication kinetics between sexes*

Day 2 post infection, we saw peak infectious virus titer in all tissue types (Figure A1). Nasal turbinate samples had the highest virus titers. Viral load began to drop in both sexes starting 4 days post infection. At day 7, almost no detectable infectious virus was detected in all tissues. None of the samples had detectable virus titer at day 14 or 28 post infection. No sex differences were observed in either peak viral load or viral clearance in all tissues.

## Discussion and Conclusion

The infectious virus titer in hamster respiratory tissues did not show sex differences. The data suggested that the difference in disease progression and severity was not caused by differential virus replication. Along with other data not included in this appendix, we have shown that male hamsters lose more body mass and suffer from more severe pulmonary pathology than female hamsters. Our data also demonstrated that virus replication and cytokine responses did not correlate with sex differences in disease severity in SCV2 infection in hamsters. Measuring antibodies from infected hamsters showed that female hamsters produced greater amounts of antibodies in both respiratory tissues and in plasma compared to males. Overall, further studies are needed to mechanistically determine why males suffers more severe outcomes compared to females in SCV2 infection.



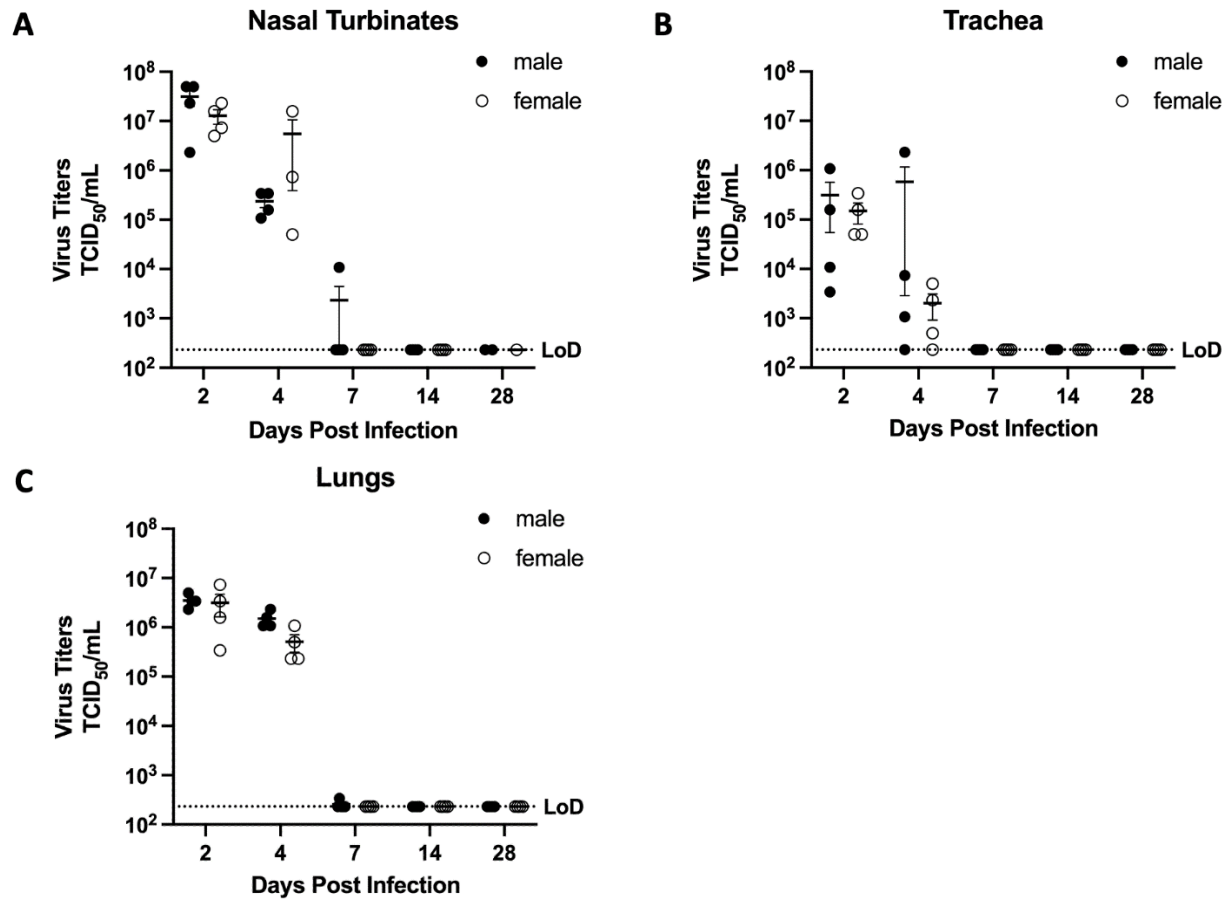


**Figure A1.** Infectious virus titers in **A** nasal turbinates, **B** trachea and **C** lungs separated by sex. Data represent mean  $\pm$  standard error of the mean from one or two experiment(s) ( $n = 1-5$ /group). Statistical analysis was done by MANOVA.

## References

1. CDC. *About Flu*. Available from: <https://www.cdc.gov/flu/about/index.html>.
2. CDC. *Key Facts About Influenza (Flu)*. Available from: <https://www.cdc.gov/flu/about/keyfacts.htm>.
3. Tokars, J.I., S.J. Olsen, and C. Reed, *Seasonal Incidence of Symptomatic Influenza in the United States*. Clin Infect Dis, 2018. **66**(10): p. 1511-1518.
4. CDC. *Disease Burden of Influenza*. Available from: <https://www.cdc.gov/flu/about/burden/index.html>.
5. CDC. *Diagnosing Flu*. Available from: <https://www.cdc.gov/flu/symptoms/testing.htm>.
6. CDC. *Rapid Influenza Diagnostic Tests*. Available from: [https://www.cdc.gov/flu/professionals/diagnosis/clinician\\_guidance\\_ridt.htm](https://www.cdc.gov/flu/professionals/diagnosis/clinician_guidance_ridt.htm).
7. CDC. *Information on Rapid Molecular Assays, RT-PCR, and other Molecular Assays for Diagnosis of Influenza Virus Infection*. Available from: <https://www.cdc.gov/flu/professionals/diagnosis/molecular-assays.htm>.
8. Sandt, C.E.v.d., et al., *Influenza B viruses: not to be discounted*. Future Microbiology, 2015. **10**(9): p. 1447-1465.
9. Vasin, A.V., et al., *Molecular mechanisms enhancing the proteome of influenza A viruses: an overview of recently discovered proteins*. Virus Res, 2014. **185**: p. 53-63.
10. Koutsakos, M., et al., *Knowns and unknowns of influenza B viruses*. Future Microbiology, 2016. **11**(1): p. 119-135.
11. Krumbholz, A., et al., *Current knowledge on PB1-F2 of influenza A viruses*. Medical Microbiology and Immunology, 2011. **200**(2): p. 69-75.
12. Gamblin, S.J. and J.J. Skehel, *Influenza hemagglutinin and neuraminidase membrane glycoproteins*. J Biol Chem, 2010. **285**(37): p. 28403-9.
13. Skehel, J.J. and D.C. Wiley, *Receptor binding and membrane fusion in virus entry: the influenza hemagglutinin*. Annu Rev Biochem, 2000. **69**: p. 531-69.
14. Gambaryan, A.S., et al., *Specification of receptor-binding phenotypes of influenza virus isolates from different hosts using synthetic sialylglycopolymers: non-egg-adapted human H1 and H3 influenza A and influenza B viruses share a common high binding affinity for 6'-sialyl(N-acetyl)lactosamine*. Virology, 1997. **232**(2): p. 345-50.
15. Samji, T., *Influenza A: understanding the viral life cycle*. Yale J Biol Med, 2009. **82**(4): p. 153-9.
16. Bouvier, N.M. and P. Palese, *The biology of influenza viruses*. Vaccine, 2008. **26 Suppl 4**(Suppl 4): p. D49-53.
17. Te Velthuis, A.J. and E. Fodor, *Influenza virus RNA polymerase: insights into the mechanisms of viral RNA synthesis*. Nat Rev Microbiol, 2016. **14**(8): p. 479-93.
18. Betakova, T., M.V. Nermut, and A.J. Hay, *The NB protein is an integral component of the membrane of influenza B virus*. J Gen Virol, 1996. **77 ( Pt 11)**: p. 2689-94.
19. Brassard, D.L., G.P. Leser, and R.A. Lamb, *Influenza B virus NB glycoprotein is a component of the virion*. Virology, 1996. **220**(2): p. 350-60.
20. Fischer, W.B., et al., *Transmembrane peptide NB of influenza B: a simulation, structure, and conductance study*. Biochemistry, 2000. **39**(41): p. 12708-16.
21. Hatta, M. and Y. Kawaoka, *The NB Protein of Influenza B Virus Is Not Necessary for Virus Replication In Vitro*. Journal of Virology, 2003. **77**(10): p. 6050-6054.
22. Francis, T., Jr., *A NEW TYPE OF VIRUS FROM EPIDEMIC INFLUENZA*. Science, 1940. **92**(2392): p. 405-8.
23. Rota, P.A., et al., *Cocirculation of two distinct evolutionary lineages of influenza type B virus since 1983*. Virology, 1990. **175**(1): p. 59-68.

24. Chen, R. and E.C. Holmes, *The evolutionary dynamics of human influenza B virus*. J Mol Evol, 2008. **66**(6): p. 655-63.
25. Hannoun, C., *The evolving history of influenza viruses and influenza vaccines*. Expert Rev Vaccines, 2013. **12**(9): p. 1085-94.
26. Vijaykrishna, D., et al., *The contrasting phylodynamics of human influenza B viruses*. Elife, 2015. **4**: p. e05055.
27. Kilbourne, E.D., *Influenza pandemics of the 20th century*. Emerg Infect Dis, 2006. **12**(1): p. 9-14.
28. Kuiken, T., et al., *Host species barriers to influenza virus infections*. Science, 2006. **312**(5772): p. 394-7.
29. Chang, C.P., et al., *Influenza virus isolations from dogs during a human epidemic in Taiwan*. Int J Zoonoses, 1976. **3**(1): p. 61-4.
30. Osterhaus, A.D., et al., *Influenza B virus in seals*. Science, 2000. **288**(5468): p. 1051-3.
31. Ran, Z., et al., *Domestic pigs are susceptible to infection with influenza B viruses*. J Virol, 2015. **89**(9): p. 4818-26.
32. Lei, N., et al., *Molecular evolution of influenza B virus during 2011-2017 in Chaoyang, Beijing, suggesting the free influenza vaccine policy*. Sci Rep, 2019. **9**(1): p. 2432.
33. Zaraket, H., et al., *Burden of influenza B virus infection and considerations for clinical management*. Antiviral Res, 2021. **185**: p. 104970.
34. Caini, S., et al., *The epidemiological signature of influenza B virus and its B/Victoria and B/Yamagata lineages in the 21st century*. PLOS ONE, 2019. **14**(9): p. e0222381.
35. CDC. *National, Regional, and State Level Outpatient Illness and Viral Surveillance*. Available from: <https://gis.cdc.gov/grasp/fluview/fluportaldashboard.html>.
36. CDC. *Past Weekly Surveillance Reports*. Available from: <https://www.cdc.gov/flu/weekly/pastreports.htm>.
37. CDC. *Age Group Distribution of Influenza Positive Specimens Reported by Public Health Laboratories*. Available from: [https://gis.cdc.gov/grasp/fluview/flu\\_by\\_age\\_virus.html](https://gis.cdc.gov/grasp/fluview/flu_by_age_virus.html).
38. CDC. *Flu Vaccines Work*. Available from: <https://www.cdc.gov/flu/vaccines-work/index.html>.
39. Barr, I.G., et al., *Cell culture-derived influenza vaccines in the severe 2017-2018 epidemic season: a step towards improved influenza vaccine effectiveness*. NPJ Vaccines, 2018. **3**: p. 44.
40. Lamb, Y.N., *Cell-Based Quadrivalent Inactivated Influenza Virus Vaccine (Flucelvax®) Tetra/Flucelvax Quadrivalent(®): A Review in the Prevention of Influenza*. Drugs, 2019. **79**(12): p. 1337-1348.
41. Rajaram, S., et al., *Influenza vaccines: the potential benefits of cell-culture isolation and manufacturing*. Ther Adv Vaccines Immunother, 2020. **8**: p. 2515135520908121.
42. Robertson, J.S., et al., *Alterations in the hemagglutinin associated with adaptation of influenza B virus to growth in eggs*. Virology, 1985. **143**(1): p. 166-74.
43. Saito, T., et al., *Antigenic alteration of influenza B virus associated with loss of a glycosylation site due to host-cell adaptation*. J Med Virol, 2004. **74**(2): p. 336-43.
44. Lugovtsev, V.Y., D.F. Smith, and J.P. Weir, *Changes of the receptor-binding properties of influenza B virus B/Victoria/504/2000 during adaptation in chicken eggs*. Virology, 2009. **394**(2): p. 218-26.
45. Lugovtsev, V.Y., et al., *Generation of the influenza B viruses with improved growth phenotype by substitution of specific amino acids of hemagglutinin*. Virology, 2007. **365**(2): p. 315-23.
46. Garretson, T.A., et al., *Identification of human vaccinees that possess antibodies targeting the egg-adapted hemagglutinin receptor binding site of an H1N1 influenza vaccine strain*. Vaccine, 2018. **36**(28): p. 4095-4101.

47. Zost, S.J., et al., *Contemporary H3N2 influenza viruses have a glycosylation site that alters binding of antibodies elicited by egg-adapted vaccine strains*. Proc Natl Acad Sci U S A, 2017. **114**(47): p. 12578-12583.
48. Abdoli, A., et al., *Comparison between MDCK and MDCK-SIAT1 cell lines as preferred host for cell culture-based influenza vaccine production*. Biotechnology Letters, 2016. **38**(6): p. 941-948.
49. Fischer, W.A., 2nd, et al., *Restricted replication of the live attenuated influenza A virus vaccine during infection of primary differentiated human nasal epithelial cells*. Vaccine, 2015. **33**(36): p. 4495-504.
50. WHO. *Recommended composition of influenza virus vaccines for use in the 2016-2017 northern hemisphere influenza season*. Available from: [https://www.who.int/influenza/vaccines/virus/recommendations/2016\\_17\\_north/en/](https://www.who.int/influenza/vaccines/virus/recommendations/2016_17_north/en/).
51. WHO. *Recommended composition of influenza virus vaccines for use in the 2017-2018 northern hemisphere influenza season*. Available from: [https://www.who.int/influenza/vaccines/virus/recommendations/2017\\_18\\_north/en/](https://www.who.int/influenza/vaccines/virus/recommendations/2017_18_north/en/).
52. WHO. *Recommended composition of influenza virus vaccines for use in the 2018-2019 northern hemisphere influenza season*. Available from: [https://www.who.int/influenza/vaccines/virus/recommendations/2018\\_19\\_north/en/](https://www.who.int/influenza/vaccines/virus/recommendations/2018_19_north/en/).
53. Ganti, K., et al., *Rab11a mediates cell-cell spread and reassortment of influenza A virus genomes via tunneling nanotubes*. bioRxiv, 2021: p. 2021.01.20.427426.
54. Sealy, J.E., et al., *Adsorptive mutation and N-linked glycosylation modulate influenza virus antigenicity and fitness*. Emerg Microbes Infect, 2020. **9**(1): p. 2622-2631.
55. Rajaram, S., et al., *Retrospective Assessment of the Antigenic Similarity of Egg-Propagated and Cell Culture-Propagated Reference Influenza Viruses as Compared with Circulating Viruses across Influenza Seasons 2002-2003 to 2017-2018*. Int J Environ Res Public Health, 2020. **17**(15).
56. Powell, H. and A. Pekosz, *Neuraminidase antigenic drift of H3N2 clade 3c.2a viruses alters virus replication, enzymatic activity and inhibitory antibody binding*. PLoS Pathog, 2020. **16**(6): p. e1008411.
57. WHO. *Recommended composition of influenza virus vaccines for use in the 2021 - 2022 northern hemisphere influenza season*. Available from: [https://www.who.int/influenza/vaccines/virus/recommendations/2021-22\\_north/en/](https://www.who.int/influenza/vaccines/virus/recommendations/2021-22_north/en/).
58. Jin, J.M., et al., *Gender Differences in Patients With COVID-19: Focus on Severity and Mortality*. Front Public Health, 2020. **8**: p. 152.
59. Meng, Y., et al., *Sex-specific clinical characteristics and prognosis of coronavirus disease-19 infection in Wuhan, China: A retrospective study of 168 severe patients*. PLoS Pathog, 2020. **16**(4): p. e1008520.
60. Peckham, H., et al., *Male sex identified by global COVID-19 meta-analysis as a risk factor for death and ITU admission*. Nat Commun, 2020. **11**(1): p. 6317.
61. GlobalHealth5050. *The Sex, Gender and COVID-19 Project*. 2020 November 30, 2020 [cited 2020 December 28]; Available from: <https://globalhealth5050.org/the-sex-gender-and-covid-19-project/>.

# Curriculum Vitae

## Ruifeng Zhou

414 Light Street 2306, Baltimore MD 21202  
+1 (949)-351-2295 | rzhou19@jhu.edu

### EDUCATION

---

**Johns Hopkins Bloomberg School of Public Health**  
*Master of Science: Molecular Microbiology and Immunology*

**Baltimore, Maryland**  
**Aug 2019 - Present**

- Cumulative GPA: 3.92
- 

**UNIVERSITY OF CALIFORNIA, IRVINE**  
*Bachelor of Science: Biological Science*

**Irvine, California**  
**Sep 2013 - Jun 2017**

- Cumulative GPA: 3.02
  - Dean's Honor List: 2017 Winter – 2017 Spring
- 

### RESEARCH EXPERIENCE

---

**Johns Hopkins Bloomberg School of Public Health**  
*Department of Molecular Microbiology and Immunology*  
**ScM student in Dr. Andrew Pekosz Lab**

**Baltimore, Maryland**  
**Nov 2019 - Present**

- Characterization and comparison of Influenza B Virus lineages.
    - Compare viral replication kinetics of IBV on MDCK-SIAT1 and hNEC culture
    - Compare plaque assay morphology of IBV on MDCK cells
    - Sequencing of IBV to identify mutations by egg and cell adaptation
  - Sex differences in SARS-CoV-2 pathogenesis in Golden Syrian Hamsters
    - SARS-CoV-2 infected hamster issue sample homogenization
    - Measure infectious virus load in hamster tissue samples
- 

**Scripps Research**  
*Genomics Core*  
**Research Technician**

**La Jolla, California**  
**Apr 2018 – Jun 2019**

- Next-generation sequencing (NGS) library preparation.
  - Droplet digital PCR operation for DNA quantification and sequence detection.
  - Tumor mutation burden analysis on FFPE samples using exome sequencing.
  - Oligonucleotides hybridization and extension on microarray printed slides.
  - Plasma stability and cell-free DNA stability test in EGFR T790M mutation detection.
- 

**Gnomegen Inc.**  
**Research Assistant**

**San Diego, California**  
**Nov 2017 – Apr 2018**

- Clinical diagnostic research.
-

- Next-generation sequencing (NGS) instrument development.
- Chip-based digital PCR assays development for tumor mutation detection, including EGFR T790M, 19 del, and multiple BRAF and KRAS mutations.
- Research project on difference in sequencing coverage and bias between PCR amplified and PCR free libraries.
- Research project using NGS platform on copy number variation (CNV) of patients with various stages, types of cancer in multiple age groups.

## INTERNSHIP EXPERIENCE

**Military Medical Research Institute of Nanjing Military Region**  
*(Internship)*

**Nanjing, China**  
**Jun 2015 - Jul 2015**

- Helped researchers with solution preparation and bacteria broth culture.
- Induced protein expression in *E. coli* using IPTG.
- Cell lysis using ultrasound and lysis buffer.
- Learned and assisted GST-tagged protein extraction and purification.
- Incubator, orbital shaker, autoclave, centrifuge, spectrometer and ultrasonic homogenizer operation.
- Experienced and learned the process of medical research.

**Bayi Hospital Affiliated Nanjing University of Chinese Medicine**  
*(Volunteer)*  
*Department of General Surgery*

**Nanjing, China**  
**Sep 2014**

- Watched and learned how department of general surgery worked in the hospital with an experienced doctor.
- The experience inspired me to grow higher responsibility and efficiency.

## EXTRA CURRICULUM

**TENDER NIGHT STUDENT CONCERT**  
*Co-founder & Studio director*

**Irvine, California**  
**Sep 2014 – Oct 2017**

- Cooperated with executive director to design and create musical performance to campus community, had held over 30 live performances.
- Technically controlled and optimized live performance quality, the size of audience had raised 10 times in 4 years.
- Led our studio group members to record and mix covers for our singers.
- Collaborated and assisted USC students to found their own student concert club (Till Dawn).

- Adaptive in bilingual environment: Mandarin (Native), English (fluent)
- Proficient in Microsoft Office
- Skilled in Image J, GraphPad, Geneious

## PUBLICATION

Zhou Ruifeng, Cai Yiran, Li Zhaoliang, Shen Shuangye, Sha Mozhou, Head Steven R., Wang Yan. A digital PCR assay development to detect EGFR T790M mutation in NSCLC patients. *Frontiers in Laboratory Medicine*. 2018;2(3):89-96. <https://doi.org/10.1016/j.flm.2018.08.002>